RM L58E08

NACA RM L58E08

RESEARCH MEMORANDUM

EXPERIMENTAL INVESTIGATION OF EFFECTS OF WING PLAN FORM

AND DIHEDRAL ANGLE ON SIDESLIP DERIVATIVES OF

SWEPTBACK-WING–BODY COMBINATIONS

AT SUPERSONIC SPEEDS

By William B. Boatright

Langley Aeronautical Laboratory
Langley Field, Va.

NATIONAL ADVISORY COMMITTEE
FOR AERONAUTICS

WASHINGTON
July 14, 1958
Declassified January 12, 1961

NATIONAL ADVISORY COMMITTEE FOR AERONAUTICS

RESEARCH MEMORANDUM

EXPERIMENTAL INVESTIGATION OF EFFECTS OF WING PLAN FORM AND DIHEDRAL ANGLE ON SIDESLIP DERIVATIVES OF SWEPTBACK-WING—BODY COMBINATIONS AT SUPERSONIC SPEEDS*

By William B. Boatright

SUMMARY

An experimental investigation of the sideslip derivatives for sweptback-wing—body combinations has been conducted at Mach numbers 1.62 and 2.62. Three wings were tested, mounted on an ogive-cylinder body, and each wing was tested at dihedral angles of about 0°, -5°, and -10°. All wings had the same area and the same taper ratio, and their mean geometric chord was located the same distance from the body nose. Two of the wings had the same sweep angle of the quarter-chord line (45°) but one had an aspect ratio of 3 and the other had an aspect ratio of 4. The third wing had an aspect ratio of 3 and a sweepback angle of the quarter-chord line of 60°.

The results showed that wing plan form and dihedral angle had little effect on the side force of the body-wing combinations and, therefore, if the side force of the body could be predicted, the side force of the combination would be well approximated. Although dihedral angle and wing plan form had little effect on the yawing moment or the directional stability parameter $C_{n_{\beta}}$, the wing contribution to this derivative was significant even at zero angle of attack and increased with increasing angle of attack.

The analysis of the rolling-moment results indicated that near zero angle of attack, for all combinations of dihedral angle and sideslip angle of the tests, the rolling moment is essentially a pure function of the difference between the geometric angle of attack of the two wing panels. However, for increasing angle of attack, effects other than geometric angle of attack become increasingly important.

---

*Title, Unclassified.

INTRODUCTION

Flight experience with supersonic aircraft has emphasized the need for better methods of estimating the lateral and directional stability derivatives of airplanes at supersonic speeds and the need for a more quantitative knowledge of the behavior of these derivatives with changes in design variables, Mach number, angle of attack, and angle of sideslip. In spite of the fact that the sideslip derivatives are among the more important derivatives which can strongly influence the motion of a flight vehicle and can be measured easily in a wind tunnel, sufficient systematic experimental investigations at supersonic speeds are not available for assessing theoretical estimating techniques. A review of available theoretical methods for estimating these derivatives is given in reference 1 and attention is drawn to the fact that, until more experimental information at supersonic speeds is available for assessing the various theories, appreciable advances in estimating techniques are unlikely. The particular phase of the problem that lies within the scope of the present investigation is the wing-body contribution to the sideslip derivatives. Experimental information is obtained for a number of sweptback-wing—body configurations for which the wing plan form and dihedral angle are varied systematically and the relative importance of the different design parameters and flight conditions on each sideslip derivative is determined. Some theoretical estimating techniques are examined and particular attention is focused on the problem of estimating C_{l_β} (the rolling moment due to sideslip). It is this derivative for which theoretical estimating techniques have had the least success at supersonic speeds (ref. 1). The analysis of the estimated results of C_{l_β} isolates angle-of-attack and dihedral-angle effects and defines the range of variables for which only the effective geometric differential angle of attack of the wing panels is important and, conversely, the range of variables for which powerful interference effects occur.

The scope of this investigation consisted of measuring the sideslip derivatives (also lift and drag) for three different sweptback-wing plan forms on an ogive-cylinder body. All the wings had the same total area and taper ratio, and the quarter-chord line of their mean geometric chord was located at the same body station. Two of the wings had the same sweep angle of the quarter-chord line but different aspect ratios, whereas the third wing had the same aspect ratio as one of the other wings but had a different sweep angle. Three different dihedral angles were tested for each wing at Mach numbers of 1.62 and 2.62.

SYMBOLS

The results are referred to the axis systems shown in figure 1. Except for the rolling moment, which is measured about the body axis, all coefficients are referenced to the wind-axis system.

A	aspect ratio
b	wing span
$\bar{c}$	wing mean geometric chord
c_r	wing root chord
c_t	wing tip chord
C_D	drag coefficient, $-X/qS$
C_L	lift coefficient, $-Z/qS$
C_l	rolling-moment coefficient, $M_{X'}/qSb$
C_{l_β}	rate of change of rolling-moment coefficient with angle of sideslip, $\partial C_l/\partial\beta$
C_n	yawing-moment coefficient, M_Z/qSb
C_n'	yawing-moment coefficient about Z'-axis (appendix A)
C_{n_β}	rate of change of yawing-moment coefficient with angle of sideslip, $\partial C_n/\partial\beta$
C_Y	side-force coefficient, F_Y/qS
C_Y'	side-force coefficient along Y'-axis (appendix A)
C_{Y_β}	rate of change of side-force coefficient with angle of sideslip, $\partial C_Y/\partial\beta$
d	body diameter (maximum)
D	drag, $-F_X$

L	lift, $-F_Z$
$M_{X'}$	moment about X'-axis
l	body length
M	Mach number
M_Z	moment about Z-axis
q	free-stream dynamic pressure
r	body radius
S	total wing area
V	free-stream velocity
F_X	force along X-axis
F_Y	force along Y-axis
F_Z	force along Z-axis
X,Y,Z	wind axes
X',Y',Z'	body axes
x_1	distance of quarter-chord point on mean geometric chord from wing apex
y_1	spanwise location of mean geometric chord from the body center line
y_e	spanwise distance from wing-body juncture to center of area of exposed panel
α	angle of attack of fuselage
α'_L	true geometric angle between plane of left panel of wing and free stream
α'_R	true geometric angle between plane of right panel of wing and free stream

β	sideslip angle, $-\psi$
Γ	dihedral angle
$\Lambda_{\bar{c}/4}$	sweep angle of quarter-chord line
Λ_{LE}	sweep angle of leading edge
Λ_{TE}	sweep angle of trailing edge
λ	wing taper ratio
ψ	angle of yaw, $-\beta$

Subscripts and abbreviations:

B	body
BW	body-wing combination

APPARATUS AND MODELS

The tests were conducted in the Langley 9-inch supersonic tunnel in which the Mach number can be varied by interchangeable nozzles. The stagnation pressure and temperature can also be controlled. Three different wing plan forms were tested on an ogive-cylinder body having a fineness ratio of 10. All wings had NACA 65A004 airfoil sections in the free-stream direction. The models were designed so that the three different wings were interchangeable and so that the quarter-chord of the mean geometric chord of each wing was the same distance from the body nose. The geometric characteristics of each wing are given in table I. It was also possible to vary dihedral angle for each wing. Figure 2(a) shows a partially exploded view of the model and a view of its various interchangeable components. A dimensional sketch of the model and its components is shown in figure 2(b).

The body housed a strain-gage balance which was used for measuring rolling moment. All other components were measured on external balances.

Transition strips (approximately 0.006 inch thick) were used near the body nose and near the wing leading edge for all tests. These strips were used to simulate the boundary-layer conditions of a high Reynolds number.

TESTS

The bent-sting technique was used in these tests. The sideslip angle was varied from -12° to 4° on each of four bent stings. The stings were bent in order to produce angles of attack of about 0°, 4°, 8°, and 12°. An optical system was used for indicating the angles of sideslip and a cathetometer was used for measuring angle of attack. Each wing dihedral angle was measured on a bench setup prior to installation in the tunnel.

The tests were conducted at Mach numbers of 1.62 and 2.62 and Reynolds number of 359,000 per inch and 402,000 per inch, respectively.

Throughout the tests the dewpoint of the tunnel air was kept sufficiently low so that the effects of moisture condensation in the tunnel test section were negligible.

PRECISION

The maximum probable errors in the individual measured quantities are estimated to be as follows:

M	± 0.01
α, deg	± 0.10
β, deg	± 0.02
Γ, deg	± 0.25
C_l	± 0.00013
C_n	± 0.0008
C_Y	± 0.0005
C_L	± 0.0007
C_D	± 0.0005

RESULTS AND DISCUSSION

Lift and Drag

The lift and drag characteristics for all the wing and body combinations which were tested are shown in figures 3 and 4, respectively. In both figures the different symbols represent results at different wing dihedral angles and the curves illustrate that the effects of wing dihedral angle on the lift and drag were essentially negligible for all wings at both test Mach numbers.

The experimental lift results are compared with the linear-theory prediction of the lift of the wing alone for each configuration in figure 3. In all cases, except for wings 1 and 2 at Mach number 2.62, the linear theory overestimates the lift. The theories of references 2 and 3 were used to calculate the theoretical lift curves and, for all the cases which are shown, the results are based on the geometry of the total wing. Although they are not shown in figure 3, the linear-theory predictions based on the exposed geometry (and referenced to the exposed geometry) were also calculated and the results were almost identical to the predictions based on the total wing plan form. If the theoretical lift results which are shown were corrected for body upwash effects, the theory would overpredict the experimental results even further except for the two cases previously mentioned. Conceivably, a theoretical prediction based on the exposed wing area but with the lift coefficient referenced to the total area and corrected for body upwash might give a better prediction of the lift curves for these configurations. However, a detailed study of the ability of theory to predict the lifts of these wings is beyond the scope of this report since the emphasis herein is on a study of the sideslip derivatives. The experimental and theoretical lifts which are shown are used later, however, in a procedure which is proposed for estimating the rolling moment due to the wing.

The drag results, which are presented in figure 4, are plotted against β for angles of attack of about 0°, 4°, 8°, and 12°. The dashed curve in each part of figure 4 represents the drag of the body alone at 0° angle of attack. The difference between the curve for the body alone and those for the body-wing combination represents the drag of the wing in the presence of the body (wing drag plus interference drag). It can be seen that for wing 3 at $M = 1.62$ (fig. 4(e)) this increment in drag coefficient due to the wing is very small for this case with the most subsonic leading edge and that at the higher Mach number of 2.62 (fig. 4(f)) the wing contribution to the drag coefficient is greater. However, the body-alone drag coefficient decreases with increasing Mach number so that the net drag coefficient of the wing-body combination is about the same at the two test Mach numbers.

Body-Alone Results

Aerodynamic characteristics in sideslip of the body alone at $\alpha = 0^\circ$ are presented in figure 5. The coefficients were referenced to the wing area, which was the same for all wings. Since the span of wing 2 was different from wings 1 and 3, the yawing-moment results are shown referenced to both spans.

The results shown in figure 5 illustrate the well-known increasing aerodynamic lifting efficiency of a body of revolution as the Mach number increases. The drag coefficient at a Mach number of 2.62 is much less than at 1.62 and the lifting efficiency (in this case C_Y) is greater at the higher Mach number. The Mach number effect on side force as predicted by the theory of reference 4 was negligible for the Mach number and Reynolds number range of the tests of this report, and, therefore, the theoretical prediction shown in figure 5 should be compared with the experimental results at both test Mach numbers. The side-force results C_Y are compared with those of the slender-body theory, the theory of reference 4, and with the experimental results of reference 5. The theory is in excellent agreement with the results at $M = 2.62$ but overestimates the side force at $M = 1.62$. The experimental side-force values of reference 5 at $M = 2.01$, which have been corrected to wind axes in figure 5, fall between the values indicated by the present tests at $M = 1.62$ and $M = 2.62$, as might be expected. The tests of reference 5 were for a wing-body combination which was almost identical to the combination with wing 2 of the present tests. The wings were identical and the moment reference point was the same proportionate distance from the body nose. However, the afterbody used for the tests of reference 5 was slightly longer and slightly boattailed. Also, transition strips were used on the body during the present tests and were not used for the tests of reference 5.

The yawing-moment results presented in figure 5 which are flagged (referenced to wing 2) should be compared with theoretical results and with the experimental results of reference 5. Apparently there is a decided effect on the yawing-moment results due to the minor differences between the body used for the present tests and the body of reference 5. The flattening of the yawing-moment curves at large negative values of β measured in this investigation was not obtained for the tests of reference 5.

Basic Sideslip Data

The variation of side-force coefficient, yawing-moment coefficient, and rolling-moment coefficient with β is shown in figures 6, 7, and 8, respectively, for the complete body-wing configurations. These data are shown for four different angles of attack and three different dihedral angles for each wing-body combination at the two test Mach numbers. Side-force and yawing-moment results of the body alone at 0° angle of attack are shown by the dashed line in each figure. The side-force and yawing-moment results are referenced to the wind-axis system, whereas the rolling-moment values are referenced to the body-axis system.

The data at 0° angle of attack in figures 6 and 7, which are compared with the body-alone results, indicate that the body is the chief contributor to the side force of the combination and that there is a significant contribution of the wing to the yawing moment of the combination.

The expected large dihedral effects on the rolling moment are illustrated in figure 8 and, although a more detailed analysis of the rolling moment is presented in a subsequent section, some linear-theory predictions of the rolling moment are shown in figures 8(c) and 8(d) for the case with 0° dihedral. The theoretical curves were calculated by the method of reference 6, which predicts a nonlinear variation of C_l with β but a linear variation of C_l with α for constant β. The theory is only shown for variations of β of $\pm 2^\circ$ since the calculation method is so laborious and since, for the cases investigated, the agreement with experiment is so poor. For wing 2 at both test Mach numbers the prediction of the variation of C_l with β at $\Gamma = 0^\circ$ is of opposite sign to the variation indicated by experiment.

Side Force and Yawing Moment of Body-Wing Combinations

The variation of C_{Y_β} with angle of attack α is shown in figure 9 for all the body-wing combinations tested. The slopes shown in this figure were taken over a range of β of $\pm 2^\circ$. In general wing dihedral has little effect on this derivative; however, a definite Mach number effect is indicated. As α is increased, C_{Y_β} becomes less negative at $M = 1.62$ and more negative at $M = 2.62$.

The variation of C_{n_β} with α is shown in figure 10. These results show essentially no effect of dihedral angle but an increase in angle of attack has a stabilizing effect on this derivative at both test Mach numbers. Since values of C_{n_β} are the same in both stability and wind axes, the C_{n_β} results of this investigation and those of reference 5 can be compared directly. This comparison is made in figure 10(b) wherein it is shown that the angle-of-attack effect on C_{n_β} is directly opposite for the two investigations; yet, aside from the difference in Mach number, only minor differences exist between the geometry of the configuration used in reference 5 and that in the present investigation. Considerable effort was expended to isolate the cause of this discrepancy in the C_{n_β} data, but the results of this effort were inconclusive. The minor differences between the geometry of the configuration of this report and that of reference 5 were: (1) the body of the model used in reference 5 had an afterbody that was 0.96 diameter longer, (2) the afterbody of the model used in reference 5 was slightly boattailed, and (3) roughness strips were used on the model in the investigation of this report and not on the model in reference 5. Although there is evidence that boattail angle can significantly affect the variation of C_n with β (compare appropriate body-alone results of ref. 7 with ref. 8), it has been shown by some subsequent tests in the Langley 4- by 4-foot supersonic pressure tunnel not to be the cause of the differences in the variation of C_{n_β} with α. These subsequent tests were made with the model of reference 5 modified to be exactly similar to the model of the present investigation. Tests with and without transition strips on this model indicated that, although the addition of transition strips produced a slight stabilizing effect on the variation of C_{n_β} with α, the effect was not sufficient to bring about agreement of the data. The thickness of these transition strips used on the model of reference 5 was scaled according to the model size of the two models. The strips were 0.006 inch thick for the present investigation, and, since the model of reference 5 was four times as large, its roughness strips were 0.024 inch thick. Additional tests were also conducted in the Langley 9-inch supersonic tunnel without transition strips and figure 11 illustrates the results of these tests. If the curves in figure 11 are compared, it can be seen that at an angle of attack of 12.40° the variation of C_n with β is only slightly less stable with the transition strips off the model. With no transition strips the C_{n_β} value at $\alpha \approx 12^\circ$ is about 0. This point is denoted in figure 10 by the flagged circular symbol.

A component breakdown of the yawing-moment results is shown in figures 12 to 17, wherein C_n is plotted against C_Y simply to illustrate both yawing-moment and side-force results on a single plot and is, of course, not intended to indicate the aerodynamic-center position. The variations of C_n with C_Y are shown for the body alone, the body-wing combination, and the body-wing combination minus the body. This last curve represents the wing contribution plus the interference between the two components. The body-alone curves, which are shown for angles of attack other than 0°, were computed from data obtained by varying β at $\alpha = 0^\circ$ by use of the technique outlined in appendix A for converting the side force to equivalent values at combined α and β. In this technique it was necessary to test the body alone at $\alpha = 0^\circ$ only. The results indicate that, in general, the wing contribution to the directional stability is significant at low angles of attack and increases as the angle of attack increases.

Figures 14 and 15 present the yawing-moment results for wing 2 and the results are compared with those of reference 5 for the zero angle-of-attack case. For this case only small differences between the wing contribution to the yawing moment are apparent in the two sets of tests. These differences might well be attributed to the experimental error and to the difference in Mach number of the tests.

Summary plots illustrating the lack of wing-plan-form effect on the yawing moment are presented in figures 18 and 19 for wings 1, 2, and 3. For the same angle of attack and Mach number, the yawing-moment results of the three wings are almost identical.

Rolling Moment

Some indication of the inability of linear theory to predict the rolling moment of these sweptback-wing—body combinations has been given by the comparison of theory and experiment shown in figures 8(c) and 8(d). Linear theory predicts that the variation of C_{l_β} with α should be linear, and for the case for which calculations were made (wing 2 at $M = 1.62$ and 2.62) it should be positive. Figure 20 shows that the experimental variation of C_{l_β} with α is negative and nonlinear. In figure 20(b) the rolling-moment data of wing 2 for 0° dihedral are compared with the results of reference 5, which were converted to the body-axis system. The data are in agreement and show essentially no Mach number effect for this particular wing. At dihedral angles other than 0° and especially for wing 3, a Mach number effect on the rolling-moment data is apparent.

The variation of C_{l_β} with dihedral angle is shown in figure 21 and indicates that this variation is more linear than the variation with angle of attack (fig. 20). Therefore, an estimate of the derivative $\partial C_{l_\beta}/\partial\Gamma$ might have more meaning and greater application than an estimate of $\partial C_{l_\beta}/\partial\alpha$. In fact, reference 5 shows that a subsonic estimate of $\partial C_{l_\beta}/\partial\Gamma$ gives good agreement for a wing identical to wing 2 at supersonic speeds. However, the data of figure 21 show that, at angles of attack other than 0°, the intercept of the slope of the curve of C_{l_β} plotted against Γ would be in doubt.

Because of the complicated geometry involved when a sweptback wing with dihedral is at a combined angle of attack and angle of sideslip, the overall assessment of the different effects on the rolling moment can be obscured. A logical question that arises is: To what extent is the rolling moment of a wing panel purely a function of the geometric angle of attack of the panel or in the case of two panels, the difference between the geometric angle of attack of these panels? Figures 22, 23, and 24 are designed to furnish the answer to this question and to indicate the range of variables for which the rolling moment might be predicted by using the experimental or theoretical lift variation with angle of attack at zero sideslip. The rolling-moment data are plotted against the difference between the true geometric angle of attack of the two wing panels (i.e., α of the left wing panel minus α of the right wing panel). A description of the derivation of the equation defining the true geometric angles of attack for combined angles of attack, angles of sideslip, and dihedral angles is given in appendix B. If the rolling moment were the sole function of this true geometric angle of attack and the corresponding lift at zero sideslip, all the data in figures 22, 23, and 24 should define a single curve. This curve would be the dot-dashed curve shown in each figure, which was computed from the experimental lift data by using the following equation:

$$C_l = \left(\frac{C_{L,BW} - C_{L,B}}{2}\right)\left(\frac{y_e + r}{b}\right) \tag{1}$$

Also shown in figures 22, 23, and 24 is the rolling-moment curve that the linear-theory lift prediction, shown in figure 3, would give as a function of the difference between the panel geometric angles of attack. This rolling moment is denoted by the dashed curve and is based on the theoretical lift and spanwise center-of-pressure location of each exposed panel.

The circular and square symbols in figures 22, 23, and 24 denote rolling-moment data near 0° angle of attack. These data define a single curve reasonably well which can be predicted by the experimental or theoretical lift results. This is especially true for the $M = 2.62$ data and the results represent rolling moment due to dihedral and sideslip in any combination. However, as the angle of attack increases, the data indicate that any prediction of the rolling moment based solely on the geometric angle of attack and the lift at zero sideslip would be grossly in error, and at high angles of attack the data for different dihedral angles no longer define a single curve as the sideslip is varied. A regular and consistent departure from the single curve defined by the experimental lifts is observed for all configurations, however, and the results suggest that the method of attack on the problem of predicting the rolling moment as exemplified by these data might lead to a reliable method of predicting the rolling moment even through the method might be partially empirical. One cause of the departure of rolling-moment results from a single curve (that is, the rolling moment at finite α minus the rolling moment at zero α for the same value of $\alpha'_L - \alpha'_R$) is wing sweep effect. For example, with the wing yawed, the effective sweepback angle of the leading edge of one panel is different from the sweepback angle of the other panel and the two panels experience different lifts. Reference 9 indicates that the sweep effect on the rolling moment can be significant, and for slender configurations which satisfy the condition that no part of the trailing edge extend forward of the region of maximum span, reference 9 shows that this sweep effect can be estimated reliably. Another probable cause of the departure of the rolling-moment results from a single curve (figs. 22, 23, and 24) is the interference effect of the body on the wing. At a negative sideslip angle, positive angle of attack, and negative dihedral angle, this increment in rolling moment due to angle of attack is positive and indicates a gain in lift on the windward panel and a loss in lift on the leeward panel. This appears reasonable; however, it is interesting to observe that this rolling-moment increment is in the opposite direction to the increment which would be predicted by simple two-dimensional crossflow considerations. Consider the following sketch which is a front view of a body-wing configuration at a negative angle of sideslip and a positive angle of attack:

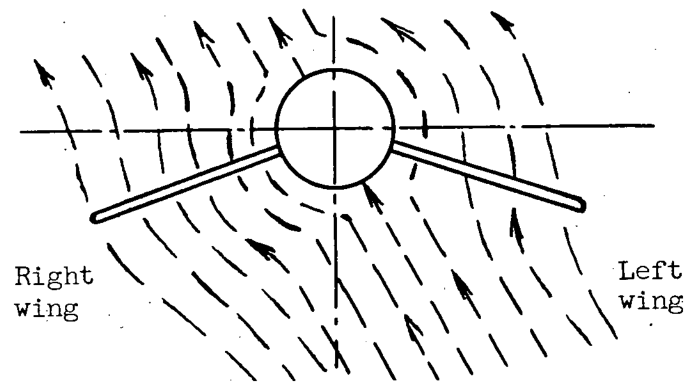

Front view

The streamlines of the flow about an infinite cylinder would be in the direction indicated by the dashed lines. Since the right wing is more nearly normal to the crossflow it would develop the most lift. Therefore, the increment in rolling moment due to the body crossflow would be negative and would be of opposite sign to the increment indicated by experiment. Figures 22, 23, and 24 emphasize the importance of these nonlinear effects since the increment in rolling moment due to effects other than geometric angle of attack are the same order of magnitude as the effects due to geometric angle of attack at model angles of attack near 12°.

CONCLUSIONS

An investigation of the sideslip derivatives for three sweptback-wing—body combinations with variable dihedral angles at Mach numbers 1.62 and 2.62 indicated the following conclusions:

1. Wing plan form and dihedral angle had only a slight effect on the side force and yawing moment of the body-wing combinations; however, a pronounced Mach number M effect on the variation of sideslip derivative C_{Y_β} with angle of attack was indicated by the data. At $M = 1.62$ increasing angle of attack caused C_{Y_β} to become less negative, and at $M = 2.62$ increasing angle of attack caused C_{Y_β} to become more negative.

2. Since only a slight contribution was made by the wing to the side force of the body-wing combination, the ability to predict the side force is chiefly determined by the ability to predict the side force on a body alone.

3. For all the wing plan forms included in this investigation, for the range of dihedral angles of the tests (as high as -10°), and for the range of sideslip angles of the tests (as high as 12°), the rolling moment at 0° angle of attack was essentially a pure function of the difference between the geometric angle of attack of the two wing panels; however, with increasing angle of attack, effects other than the geometric angle of attack became increasingly important and at 12° model angle of attack the rolling moment, due to these other effects, was as large as the rolling moment produced by the difference between the geometric angle of attack of the two wing panels.

4. The rolling moment can be predicted readily for cases in which it is essentially a pure function of the difference between the geometric angle of attack of the two wing panels (i.e., combined angle of sideslip and dihedral angle); however, further theoretical work appears to be needed in order to predict the rolling moment when angle-of-attack effects must also be considered.

Langley Aeronautical Laboratory,
National Advisory Committee for Aeronautics,
Langley Field, Va., April 16, 1958.

APPENDIX A

METHOD OF CONVERTING THE BODY-ALONE RESULTS SHOWING THE VARIATION OF C_Y OR C_n WITH β AT $\alpha = 0^{\circ}$ TO EQUIVALENT RESULTS AT COMBINED ANGLES OF ATTACK AND SIDESLIP

In sketch 1, consider the X'-axis as representing the body axis of a circular body and the X-axis as representing a line parallel to the free-stream direction.

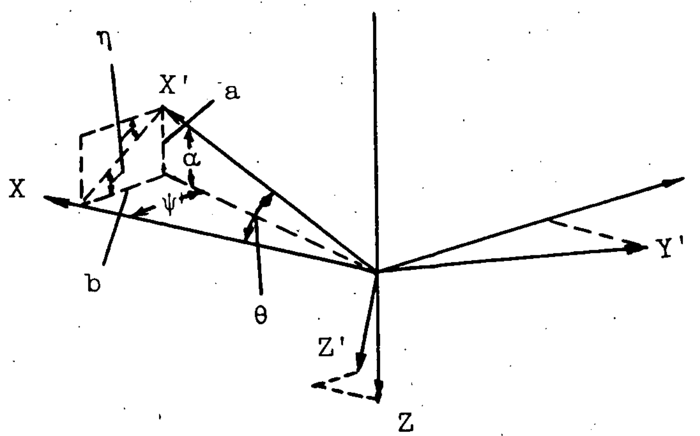

Sketch 1

When the body is at a combined α and β, it can correspond to the equivalent case of a body at an angle ψ which is equal to θ, but for which $\alpha = 0^{\circ}$. The relations between α, ψ, θ, and η are as follows:

$$\cos\theta = \cos\alpha\cos\psi \tag{A1}$$

$$\eta = \tan^{-1}\frac{a}{b} \tag{A2}$$

where

$$a = \sin\alpha\cos\beta$$

and

$$b = \cos \alpha \sin \psi$$

$$\tan \eta = \frac{\tan \alpha}{\sin \psi} \tag{A3}$$

With reference to sketch 1, if the measured side force is in the plane of θ, it can be corrected to the plane of ψ by the relation

$$C_Y = C_Y' \cos \eta \tag{A4}$$

or similarly the yawing moment can be converted by the relation

$$C_n = C_n' \cos \eta \tag{A5}$$

Therefore, knowing the variation of C_Y with ψ (or β) or C_n with ψ at $\alpha = 0^\circ$ corresponds to knowing the variation with θ in sketch 1, and the values can be converted to equivalent combined angles of attack and sideslip by using the foregoing formulas.

APPENDIX B

DERIVATION OF THE FORMULA FOR THE EFFECTIVE GEOMETRIC

ANGLE OF ATTACK OF A WING PANEL WITH DIHEDRAL IN

COMBINED ANGLE OF ATTACK AND SIDESLIP

The problem considered herein is the determination of the true geometric angle of attack of a wing panel at a combined angle of attack, angle of yaw or sideslip, and dihedral angle. This true geometric angle of attack is the angle between the plane of the wing and the free-stream direction and, for the general case, it is different for each wing panel. Approximate expressions for this angle have been published in references 10 and 11.

The orientation of the axes is shown in sketch 2.

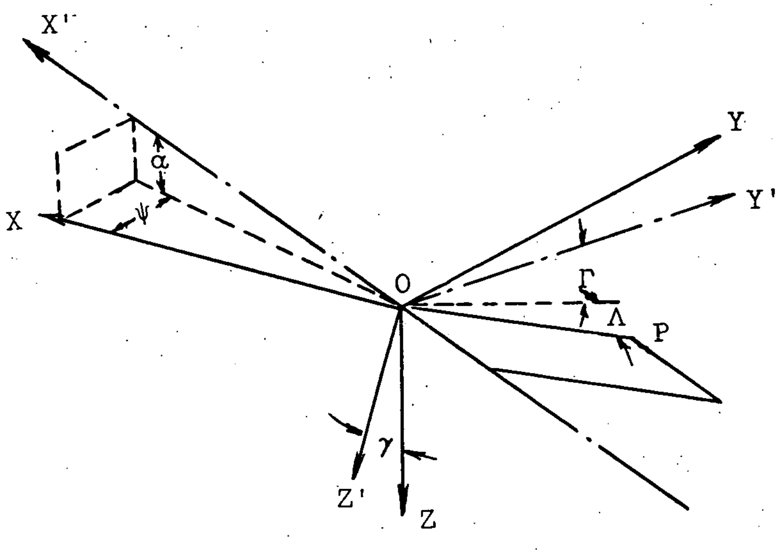

Sketch 2

In this sketch X, Y, and Z should be considered wind axes and X', Y', and Z' should be considered body axes for a configuration at an angle of attack α and an angle of yaw ψ. The line OP represents a line lying in the plane of the wing. It might be considered the leading edge of a sweptback wing, although it can be readily seen that the angle between the plane of the wing and the free-stream direction is independent of the sweepback angle which is measured in the plane of the wing.

With reference to sketch 2 which shows the relation between the body axes and the wind axes, the direction cosines of OX', OY', and OZ' with respect to OX, OY, and OZ are as follows:

$$\left.\begin{aligned}
l_1 &\equiv \cos X'OX = \cos\alpha \cos\psi \\
m_1 &\equiv \cos X'OY = \cos\alpha \sin\psi \\
n_1 &\equiv \cos X'OZ = -\sin\alpha \\
l_2 &\equiv \cos Y'OX = -\sin\psi \\
m_2 &\equiv \cos Y'OY = \cos\psi \\
n_2 &\equiv \cos Y'OZ = 0 \\
l_3 &\equiv \cos Z'OX = \sin\alpha \cos\psi \\
m_3 &\equiv \cos Z'OY = \sin\alpha \sin\psi \\
n_3 &\equiv \cos Z'OZ = \cos\alpha
\end{aligned}\right\} \tag{B1}$$

Since the wing geometry is always specified with respect to the body axes, the equation for the plane of the wing is determined in terms of the X'-, Y'-, and Z'-axes and the effective angle of attack of each wing panel is found by solving for the angle between the intercept of this plane and the XZ-plane.

Sketch 3 shows the relation of the lines OP and OQ with respect to the X'-, Y'-, and Z'-axes.

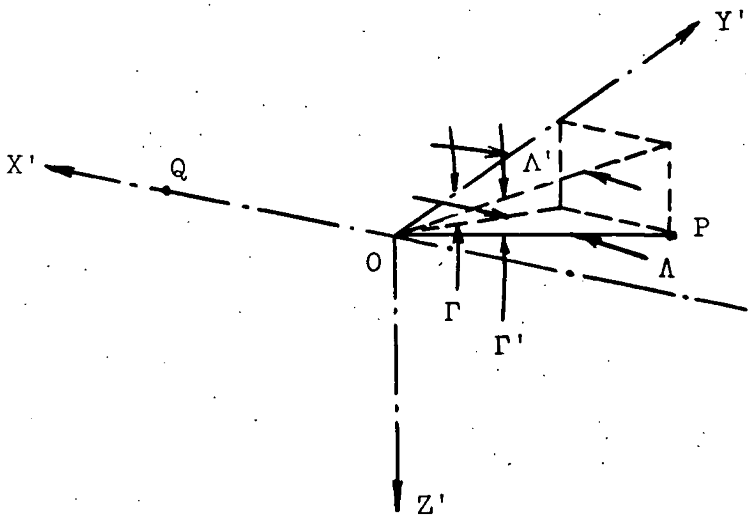

Sketch 3

The wing dihedral angle is Γ and the sweepback angle of a line lying in the plane of the wing is Λ; Λ' is the projection of Λ onto the $X'Y'$-plane and Γ' is the dihedral angle in the plane POZ'. The direction cosines of OP with respect to X', Y', and Z' are as follows:

$$\left.\begin{aligned} l_4 &= -\cos\Gamma'\sin\Lambda' = -\sin\Lambda \\ m_4 &= \cos\Gamma'\cos\Lambda' = \cos\Lambda\cos\Gamma \\ n_4 &= \sin\Gamma' = \cos\Lambda\sin\Gamma \end{aligned}\right\} \tag{B2}$$

Since the cosine of the angle between two intersecting lines is the sum of the products of their direction cosines, the direction cosines of OP with respect to OX, OY, and OZ, respectively, are as follows:

$$
\left.
\begin{aligned}
l_5 &= l_1 l_4 + l_2 m_4 + l_3 n_4 = -\cos\alpha\cos\psi\sin\Lambda - \sin\psi\cos\Lambda\cos\Gamma + \\
&\quad \sin\alpha\cos\psi\sin\Gamma\cos\Lambda \\
m_5 &= m_1 l_4 + m_2 m_4 + m_3 n_4 = -\cos\alpha\sin\psi\sin\Lambda + \cos\psi\cos\Lambda\cos\Gamma + \\
&\quad \sin\alpha\sin\psi\cos\Lambda\sin\Gamma \\
n_5 &= n_1 l_4 + n_2 m_4 + n_3 n_4 = \sin\alpha\sin\Lambda + 0 + \cos\alpha\cos\Lambda\sin\Gamma
\end{aligned}
\right\} \tag{B3}
$$

If the point P is assumed to be a unit distance from the origin O, then the coordinates of P are:

$$
\left.
\begin{aligned}
X_P &= l_5 \\
Y_P &= m_5 \\
Z_P &= n_5
\end{aligned}
\right\} \tag{B4}
$$

If the point Q, located on the X'-axis is assumed to be a unit distance from the origin, then the coordinates of Q are:

$$
\left.
\begin{aligned}
X_Q &= l_1 \\
Y_Q &= m_1 \\
Z_Q &= n_1
\end{aligned}
\right\} \tag{B5}
$$

The three points P, Q, and O are in the plane of the wing. The equation for this plane with respect to the X, Y, and Z axes is determined as follows:

General equation of all planes through origin,

$$AX + BY + CZ = 0 \tag{B6}$$

Equation for planes through P and O,

$$Al_5 + Bm_5 + Cn_5 = 0 \tag{B7}$$

Equation for planes through Q and O,

$$Al_1 + Bm_1 + Cn_1 = 0 \tag{B8}$$

and from equations (B7) and (B8),

$$\left.\begin{aligned} C &= \frac{B\left(m_1 l_5 - m_5 l_1\right)}{n_5 l_1 - n_1 l_5} \\ A &= \frac{B\left(m_5 n_1 - m_1 n_5\right)}{l_1 n_5 - l_5 n_1} \end{aligned}\right\} \tag{B9}$$

Therefore, the equation for the plane of the wing is

$$\frac{\left(m_5 n_1 - m_1 n_5\right)}{\left(l_1 n_5 - l_5 n_1\right)} X + Y + \frac{\left(m_1 l_5 - m_5 l_1\right)}{\left(n_5 l_1 - n_1 l_5\right)} = 0 \tag{B10}$$

Since the intercept of this plane with the XZ-plane is found by letting $Y = 0$, the angle between the intercept and the X-axis, which is the true geometric angle of attack of the wing, is

$$\tan \alpha' = \frac{-Z}{X} = -\left(\frac{m_1 n_5 - m_5 n_1}{m_1 l_5 - m_5 l_1}\right) \tag{B11}$$

This equation reduces to

$$\tan \alpha' = \tan \alpha \cos \psi + \frac{\sin \psi \tan \Gamma}{\cos \alpha} \tag{B12a}$$

or

$$\tan \alpha' = \tan \alpha \cos \beta - \frac{\sin \beta \tan \Gamma}{\cos \alpha} \tag{B12b}$$

REFERENCES

1. Watts, P. E.: Notes on the Estimation of Aircraft Lateral Stability Derivatives at Supersonic Speeds. Tech. Note No. Aero.2414, British R.A.E., Nov. 1955.

2. Cohen, Doris: Formulas for the Supersonic Loading, Lift, and Drag of Flat Swept-Back Wings With Leading Edges Behind the Mach Lines. NACA Rep. 1050, 1951.

3. Harmon, Sidney M., and Jeffreys, Isabella: Theoretical Lift and Damping in Roll of Thin Wings With Arbitrary Sweep and Taper at Supersonic Speeds - Supersonic Leading and Trailing Edges. NACA TN 2114, 1950.

4. Allen, H. Julian, and Perkins, Edward W.: A Study of Effects of Viscosity on Flow Over Slender Inclined Bodies of Revolution. NACA Rep. 1048, 1951. (Supersedes NACA TN 2044.)

5. Spearman, M. Leroy: Investigation of the Aerodynamic Characteristics in Pitch and Sideslip of a 45° Sweptback-Wing Airplane Model With Various Vertical Locations of the Wing and Horizontal Tail - Effect of Wing Location and Geometric Dihedral for the Wing-Body Combination, M = 2.01. NACA RM L55B18, 1955.

6. Margolis, Kenneth, Sherman, Windsor L., and Hannah, Margery E.: Theoretical Calculation of the Pressure Distribution, Span Loading, and Rolling Moment Due to Sideslip at Supersonic Speeds for Thin Sweptback Tapered Wings With Supersonic Trailing Edges and Wing Tips Parallel to the Axis of Wing Symmetry. NACA TN 2898, 1953.

7. Grigsby, Carl E.: Tests at Mach Number 1.62 of a Series of Missile Configurations Having Tandem Cruciform Lifting Surfaces. NACA RM L51J15, 1952.

8. Grigsby, Carl E.: An Investigation at Mach Numbers of 1.62 and 1.93 of the Lift Effectiveness and Integrated Downwash Characteristics of Several In-Line Missile Configurations Having Equal-Span Wings and Tails. NACA RM L52A02, 1952.

9. Spahr, J. Richard: Contribution of the Wing Panels to the Forces and Moments of Supersonic Wing-Body Combinations at Combined Angles. NACA TN 4146, 1958.

10. Levacic, I.: Rolling Moment Due to Sideslip. Part I. The Effect of Dihedral. Rep. No. Aero.2028, British R.A.E., Apr. 1945.

11. Purser, Paul E., and Campbell, John P.: Experimental Verification of a Simplified Vee-Tail Theory and Analysis of Available Data on Complete Models With Vee Tails. NACA Rep. 823, 1945. (Supersedes NACA ACR L5A03.)

TABLE I

GEOMETRIC CHARACTERISTICS OF MODELS

(BASED ON INCLUDED AREA)

Ogive-cylinder body:

Diameter, ft	0.0625
Nose fineness ratio	3.5
Body fineness ratio	10
Ogive radius of curvature, ft	0.781

Wings:	Wing 1	Wing 2	Wing 3
Airfoil section (streamwise)	NACA 65A004	NACA 65A004	NACA 65A004
Aspect ratio	3	4	3
$\Lambda_{\bar{c}/4}$, deg	45	45	60
Λ_{LE}, deg	50.71	49.40	62.90
Λ_{TE}, deg	18.49	26.57	46.81
λ	0.2	0.2	0.2
S, sq ft	0.0506	0.0506	0.0506
$\bar{c}$, ft	0.149	0.129	0.149
c_r, ft	0.216	0.187	0.216
b/2, ft	0.195	0.225	0.195
x_1, ft	0.093	0.102	0.148
y_1, ft	0.076	0.087	0.076

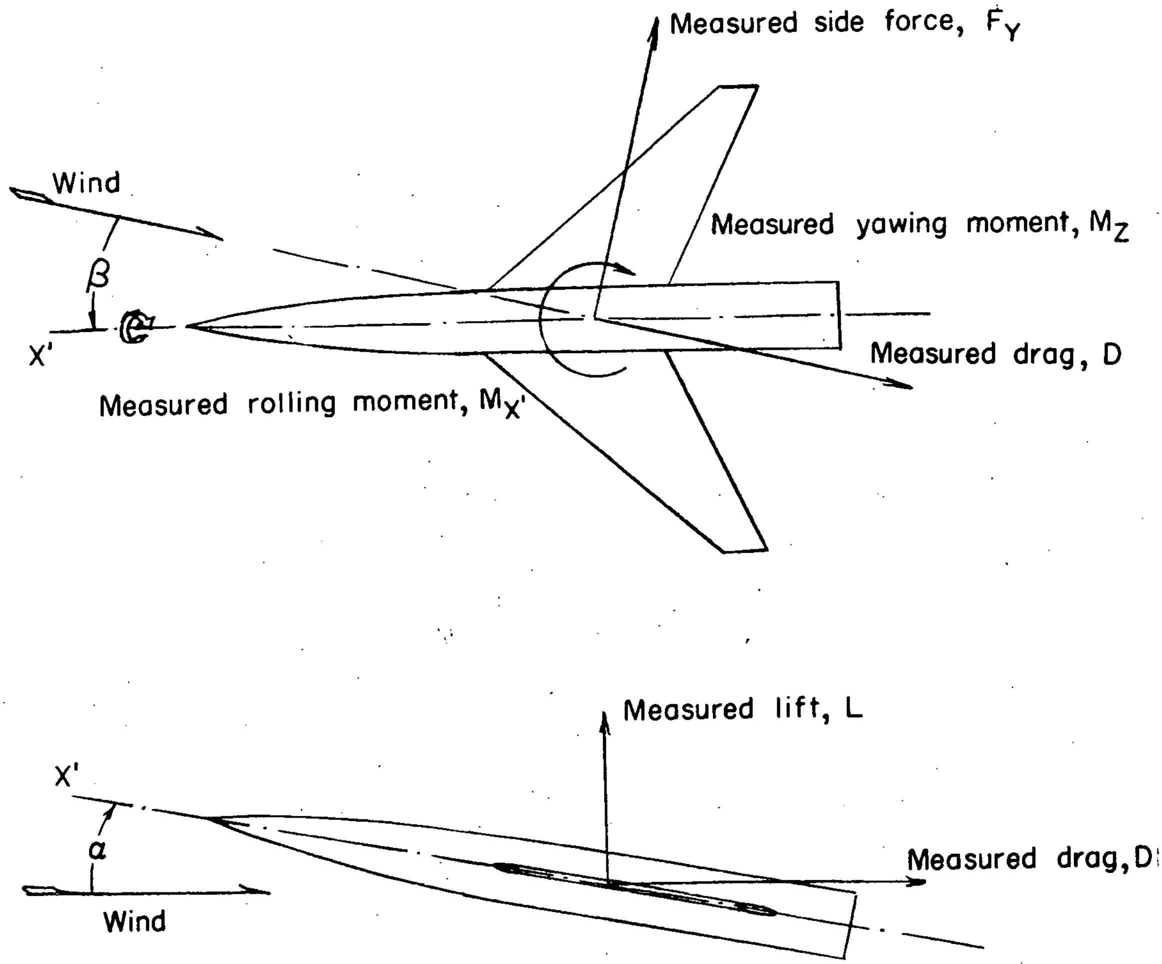

Figure 1.- Systems of axes used in data presentation. Notice that all measured forces and moments are in wind-axis system except for the rolling moment.

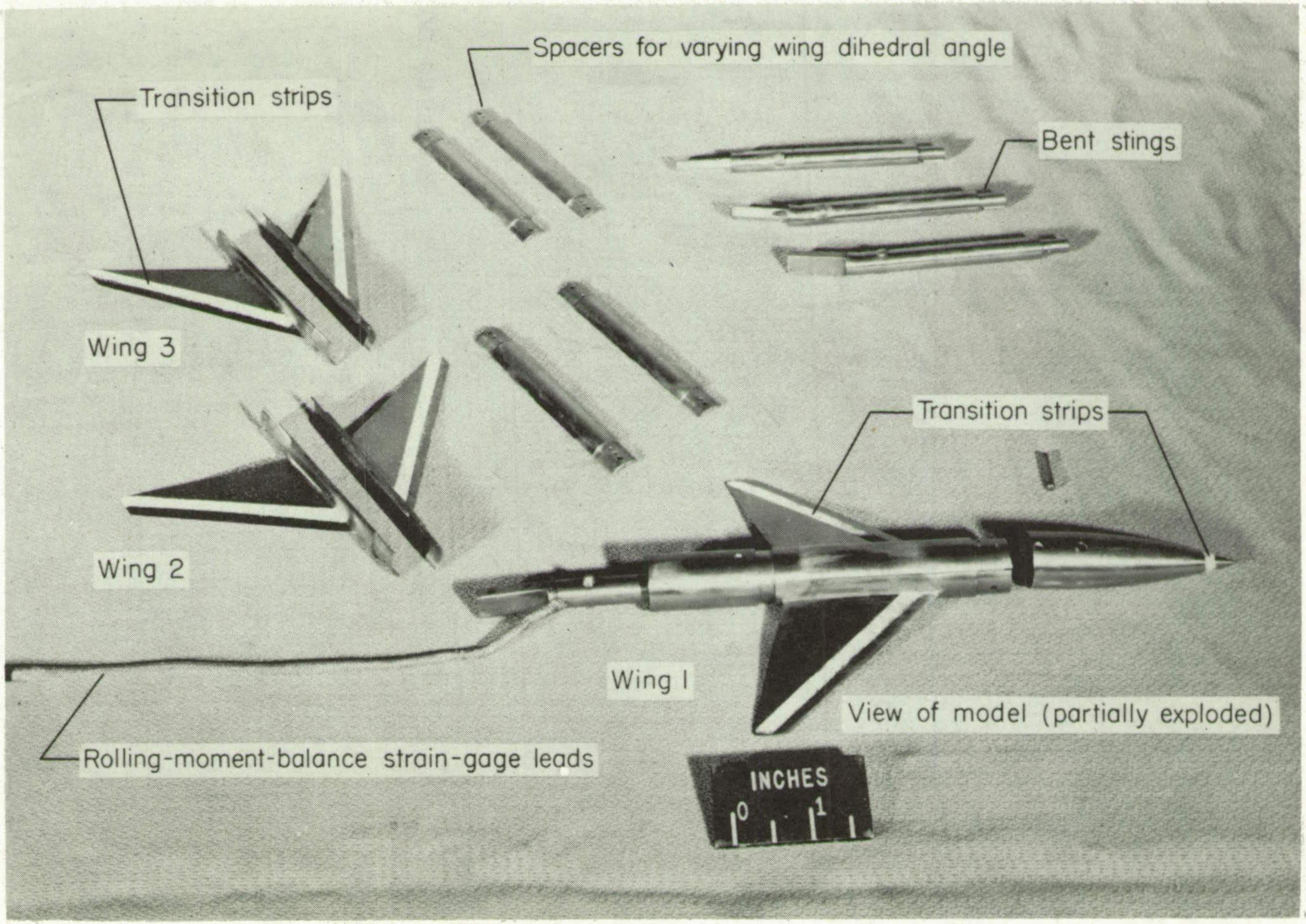

L-94648.1

(a) Wings and ogive-cylinder body used in investigation.

Figure 2.- Component parts of models.

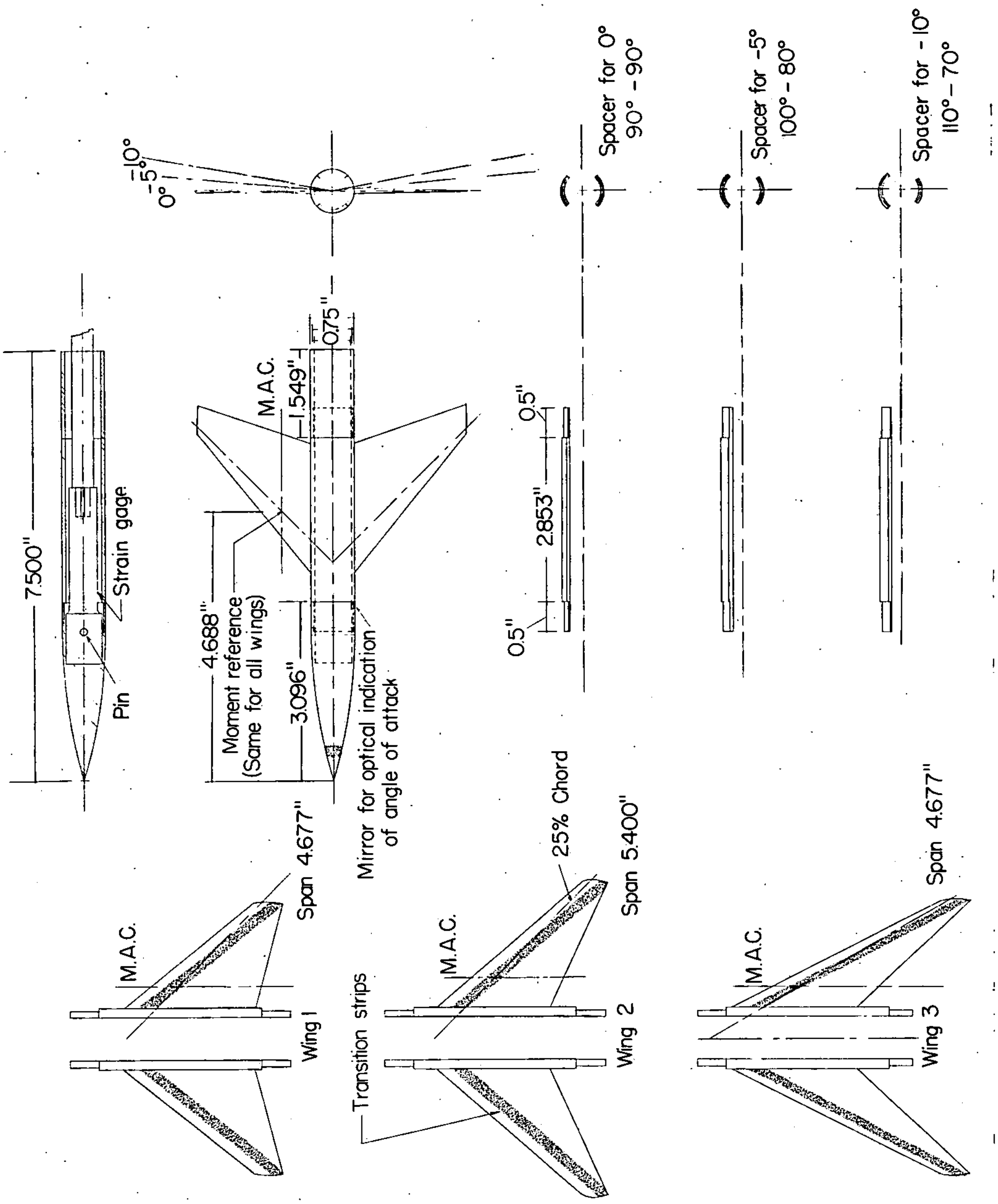

(b) Dimensional sketch of model and its components.

Figure 2.- Concluded.

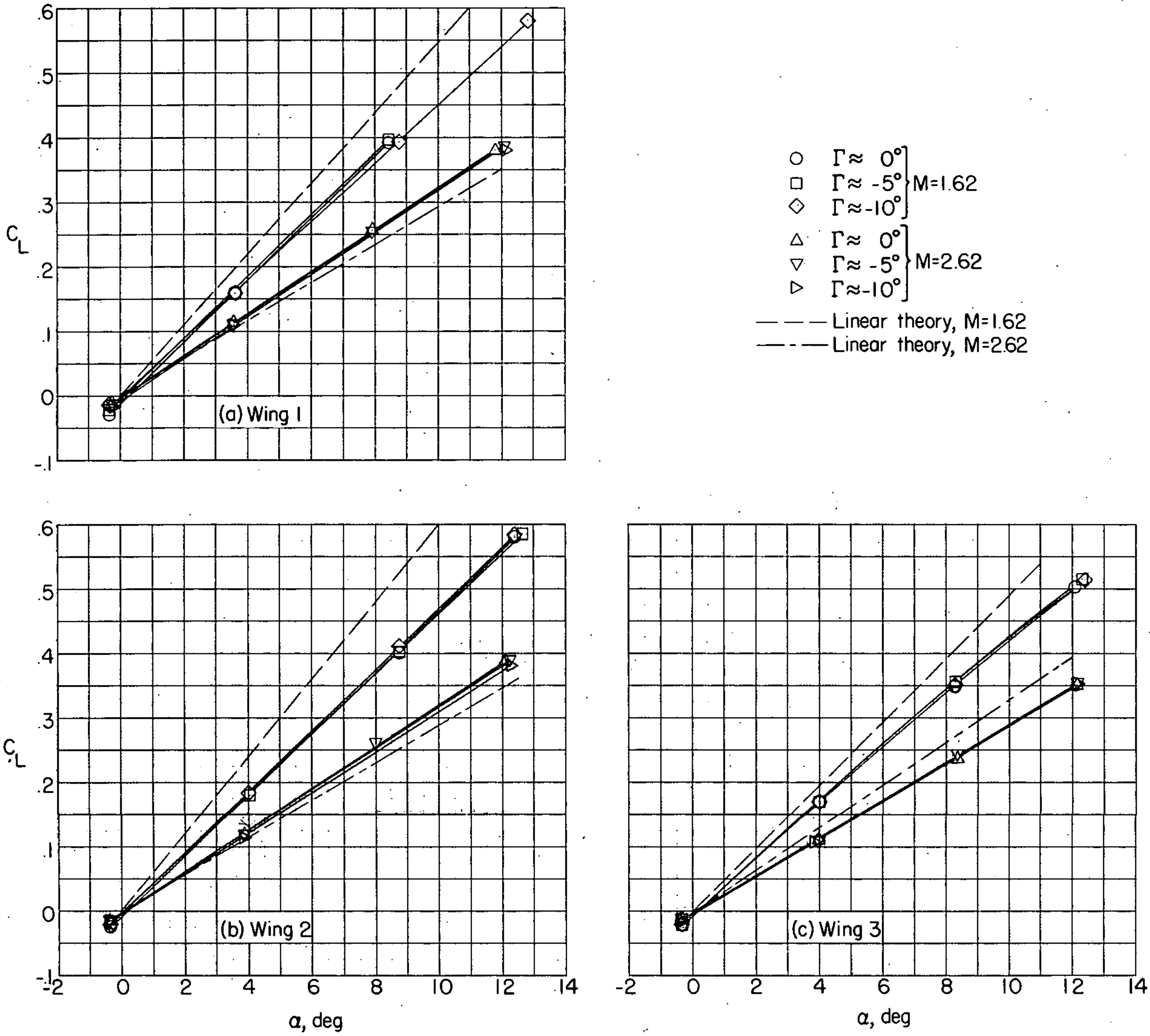

Figure 3.- Lift characteristics of wing-body combinations.

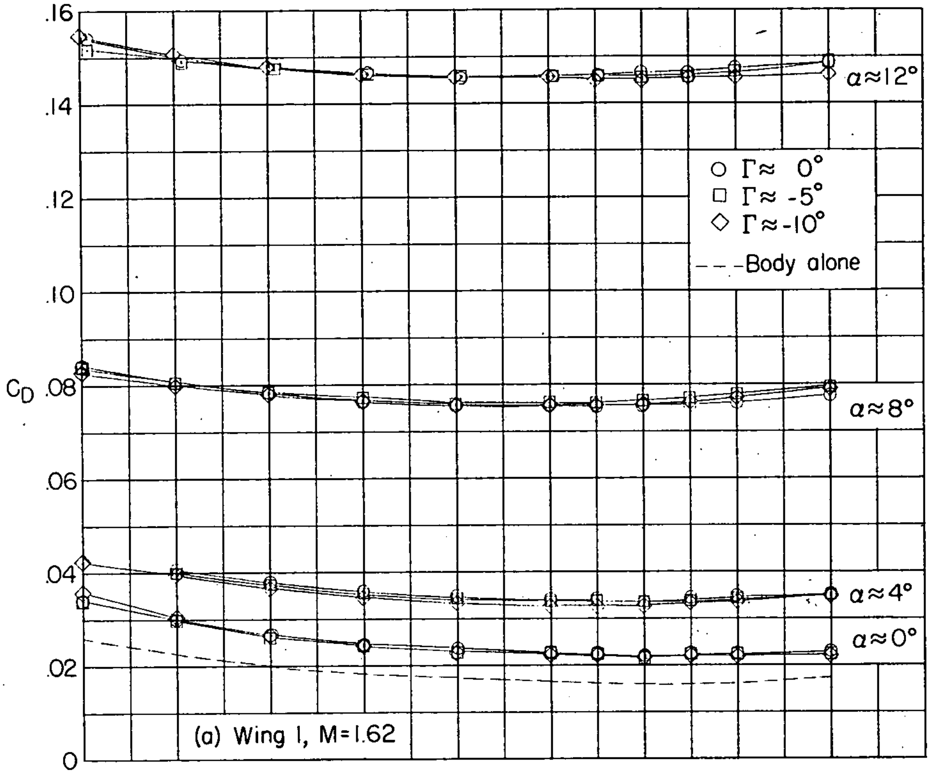

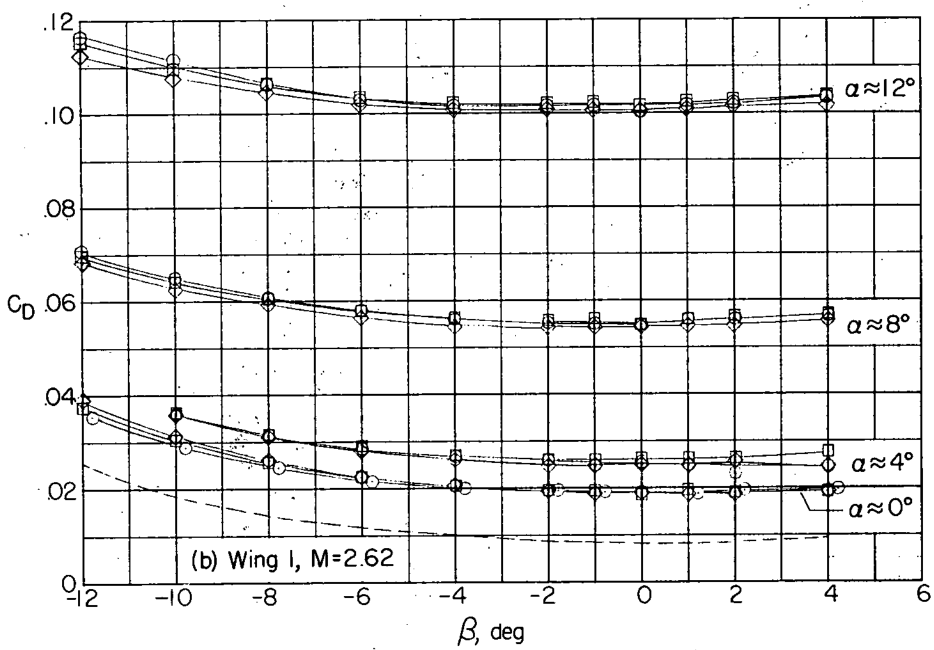

Figure 4.- Drag characteristics of wing-body combinations.

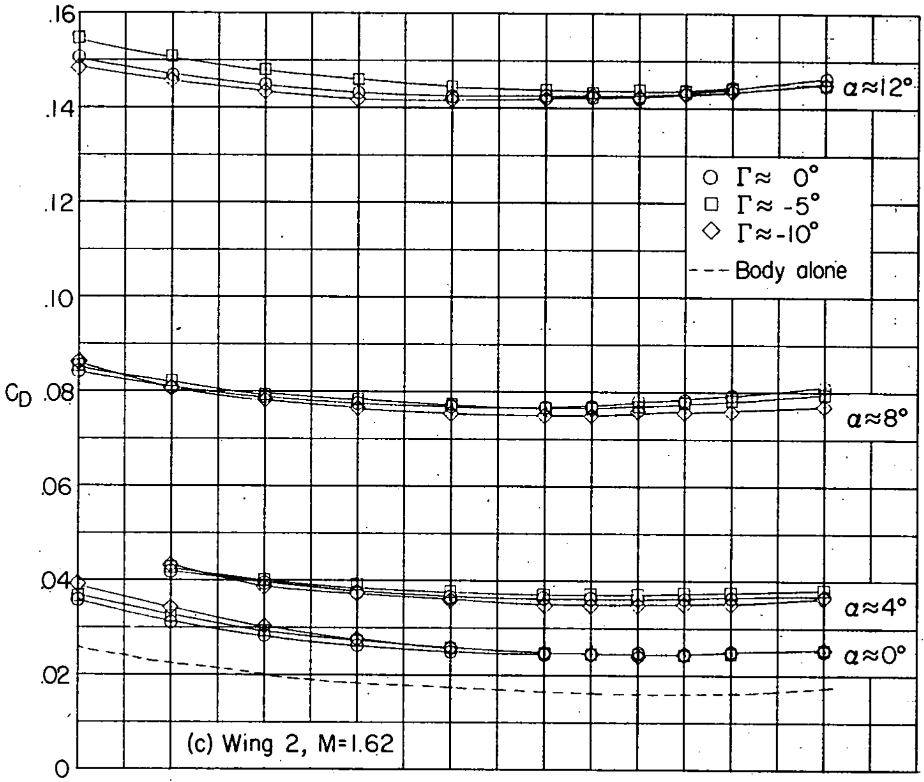

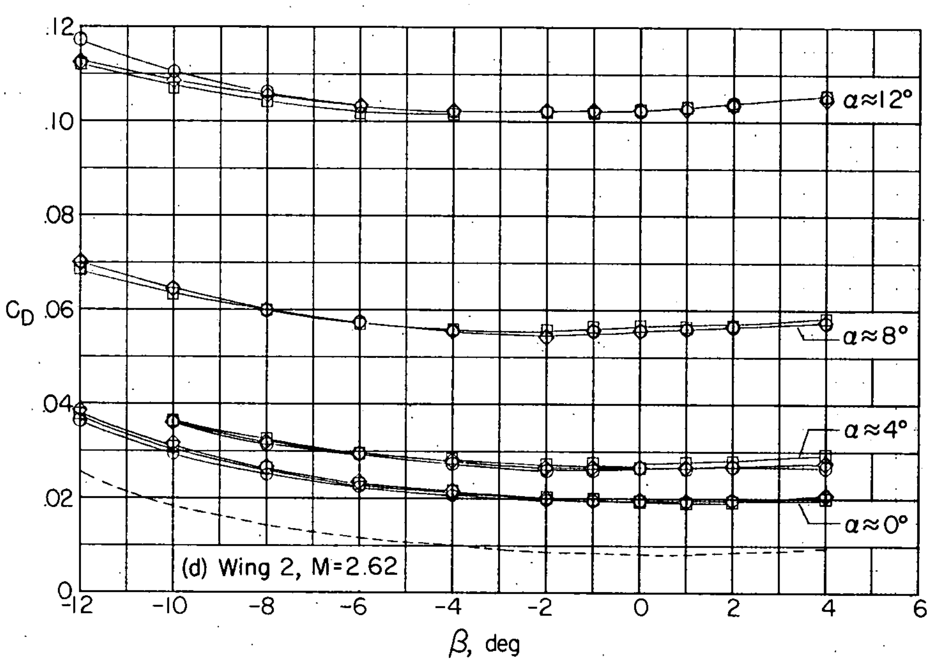

Figure 4.- Continued.

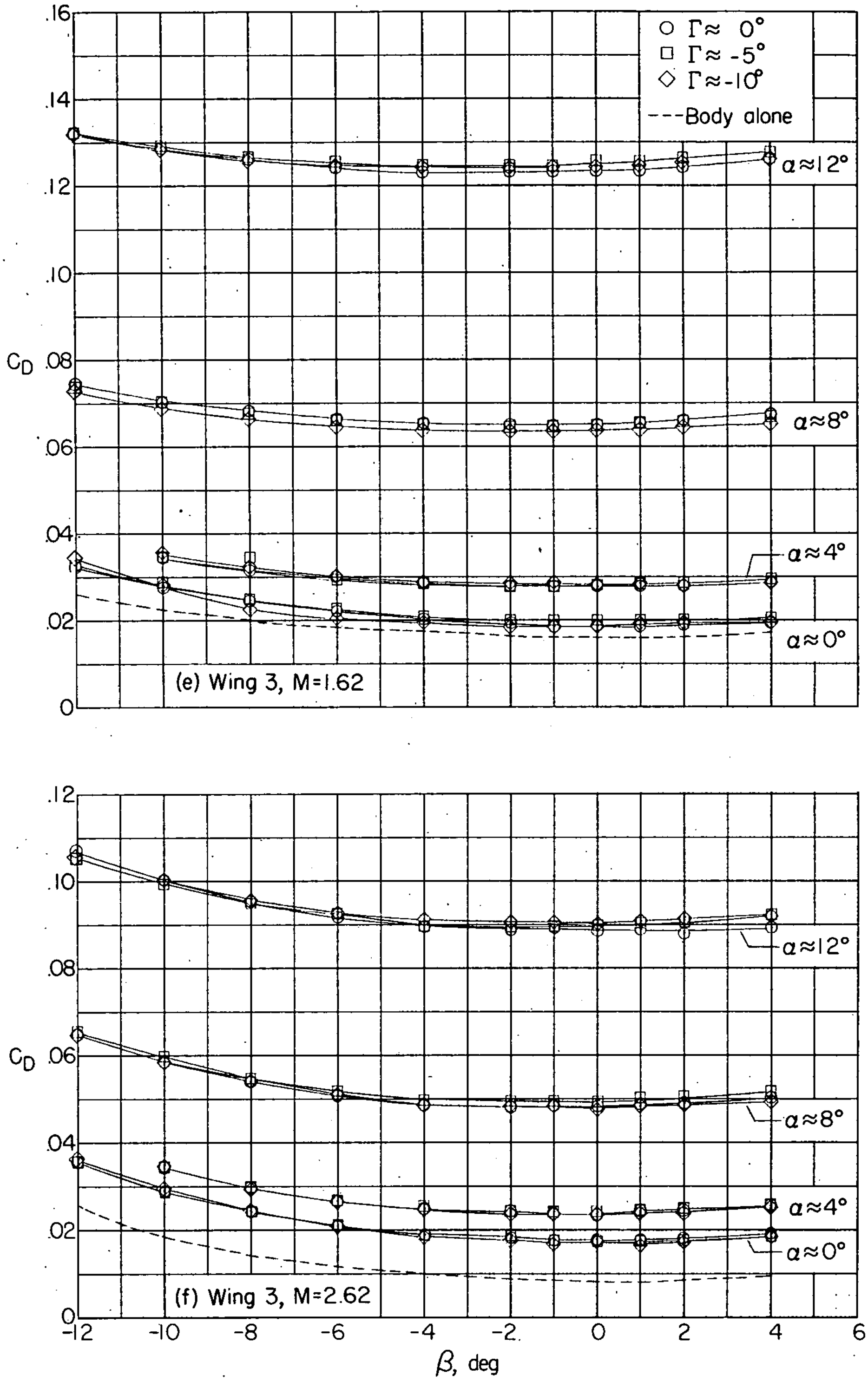

Figure 4.- Concluded.

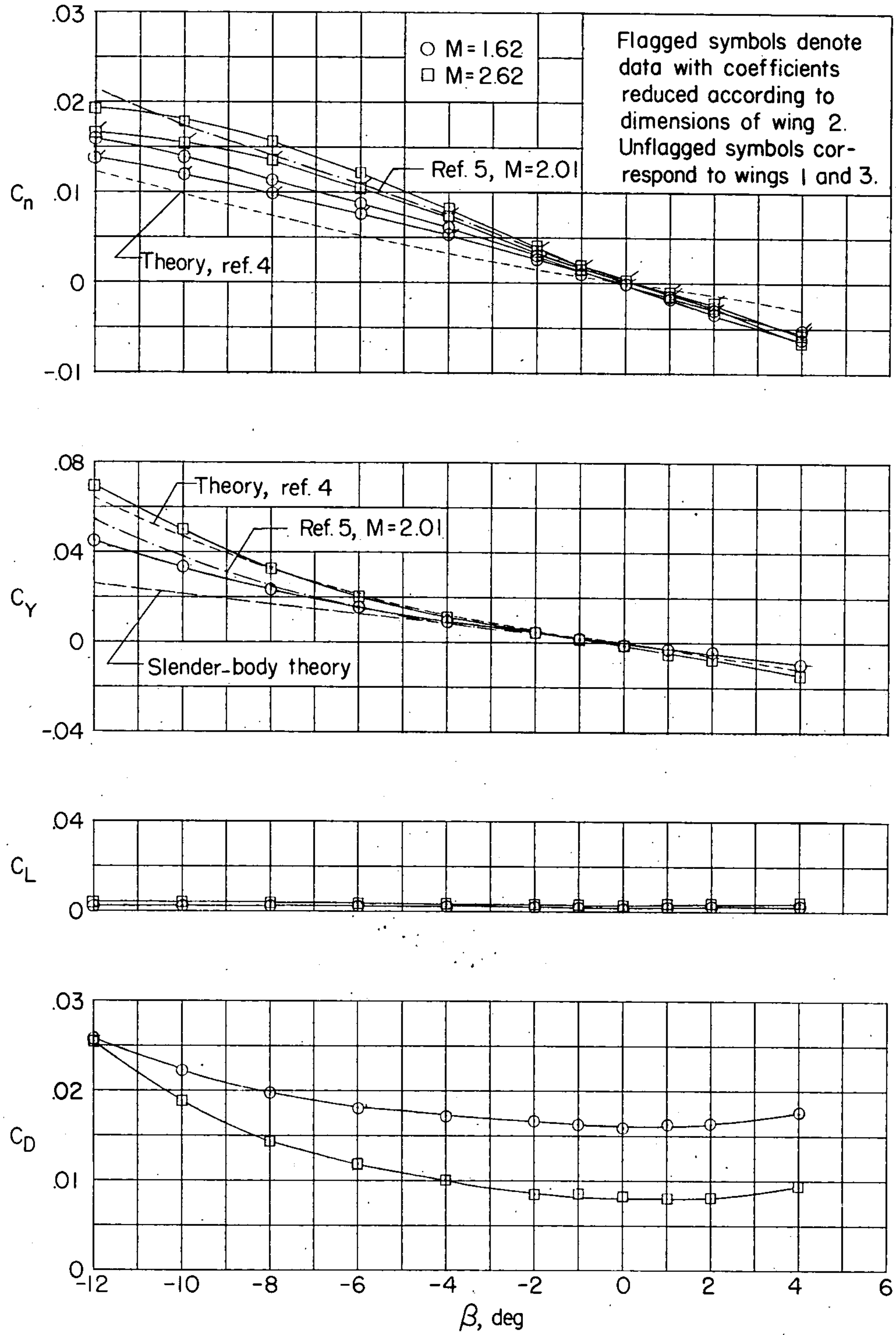

Figure 5.- Aerodynamic characteristics in sideslip of body alone.

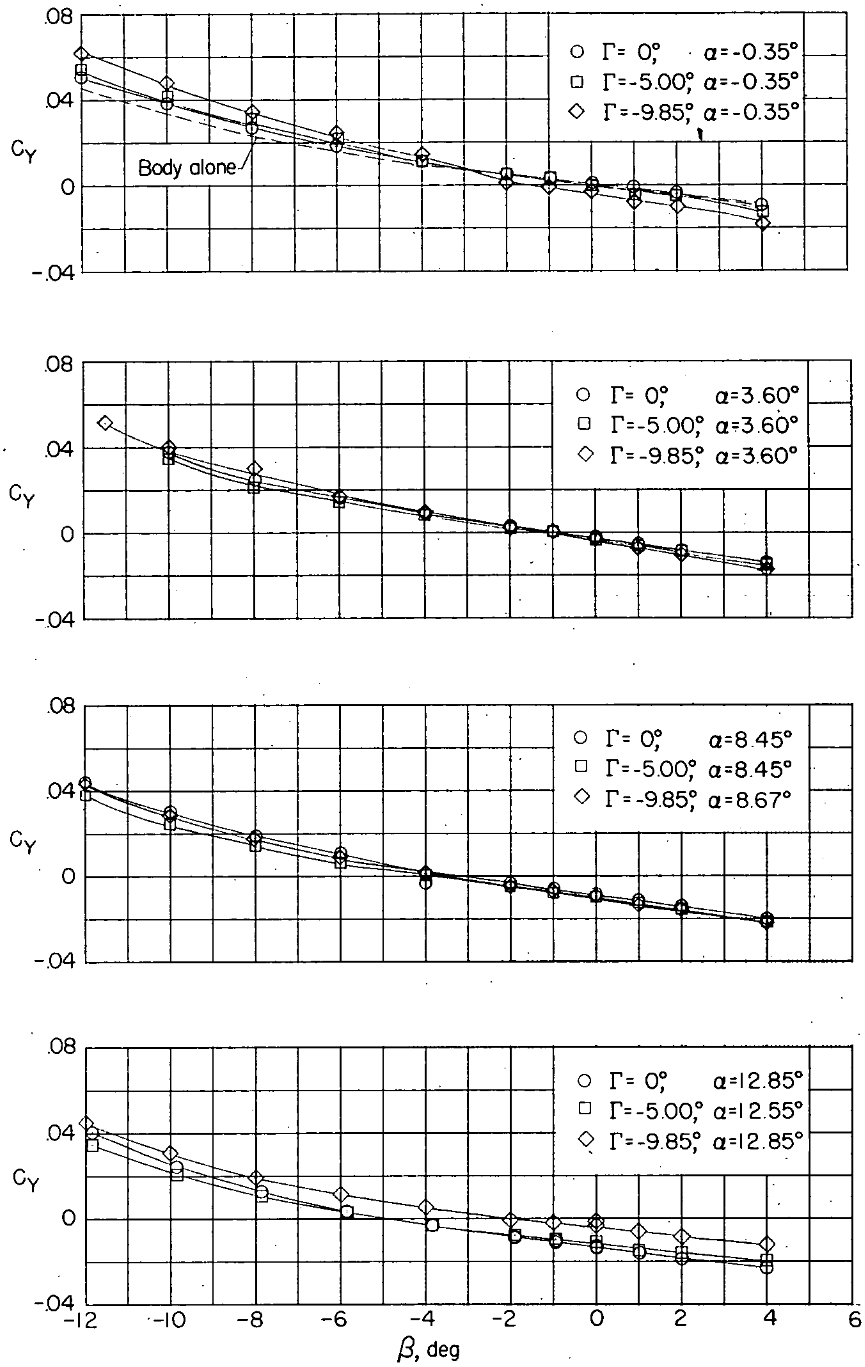

(a) Wing 1 at M = 1.62.

Figure 6.- Side-force characteristics of wing-body combinations. (Wind-axis system.)

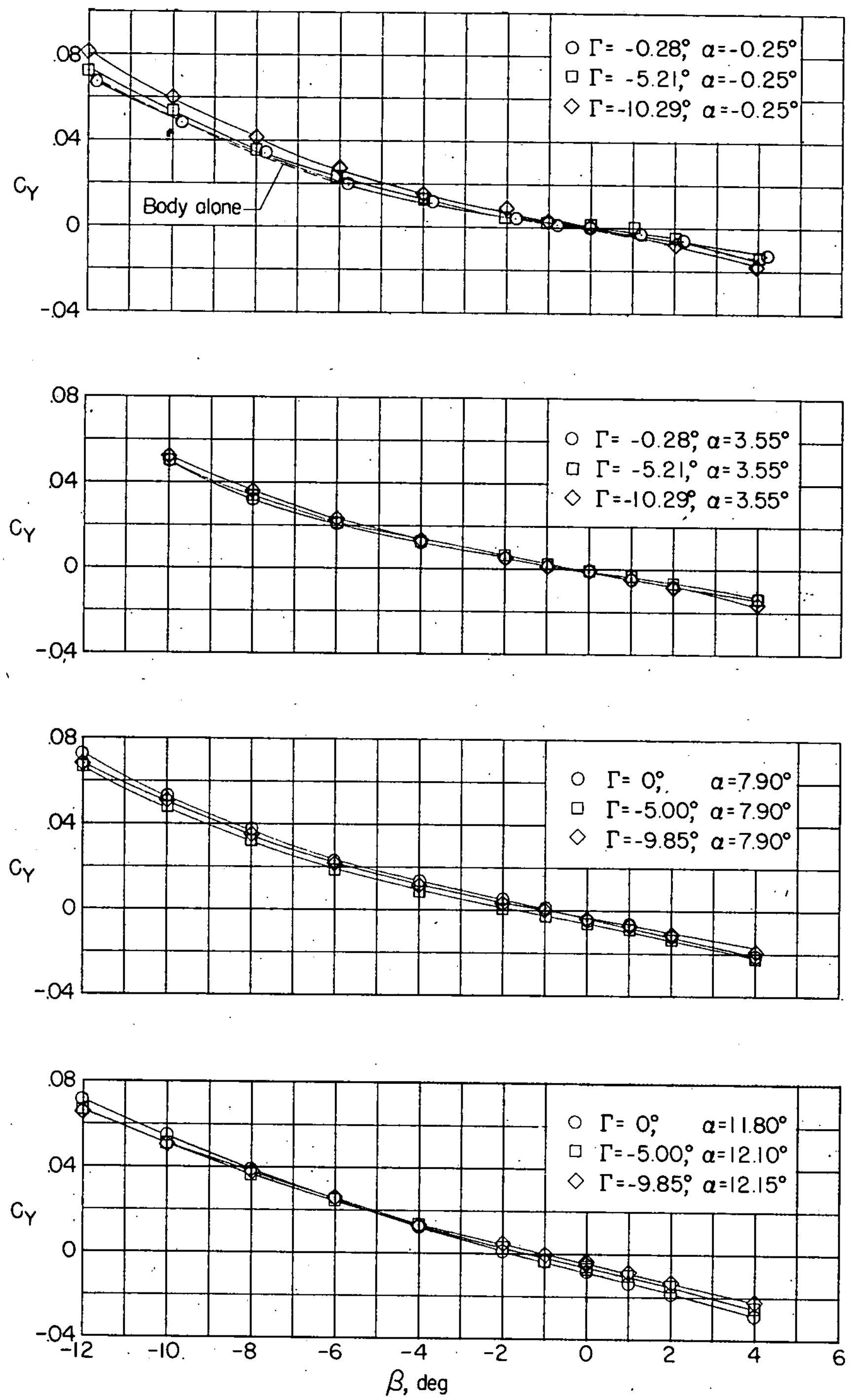

(b) Wing 1 at M = 2.62.

Figure 6.- Continued.

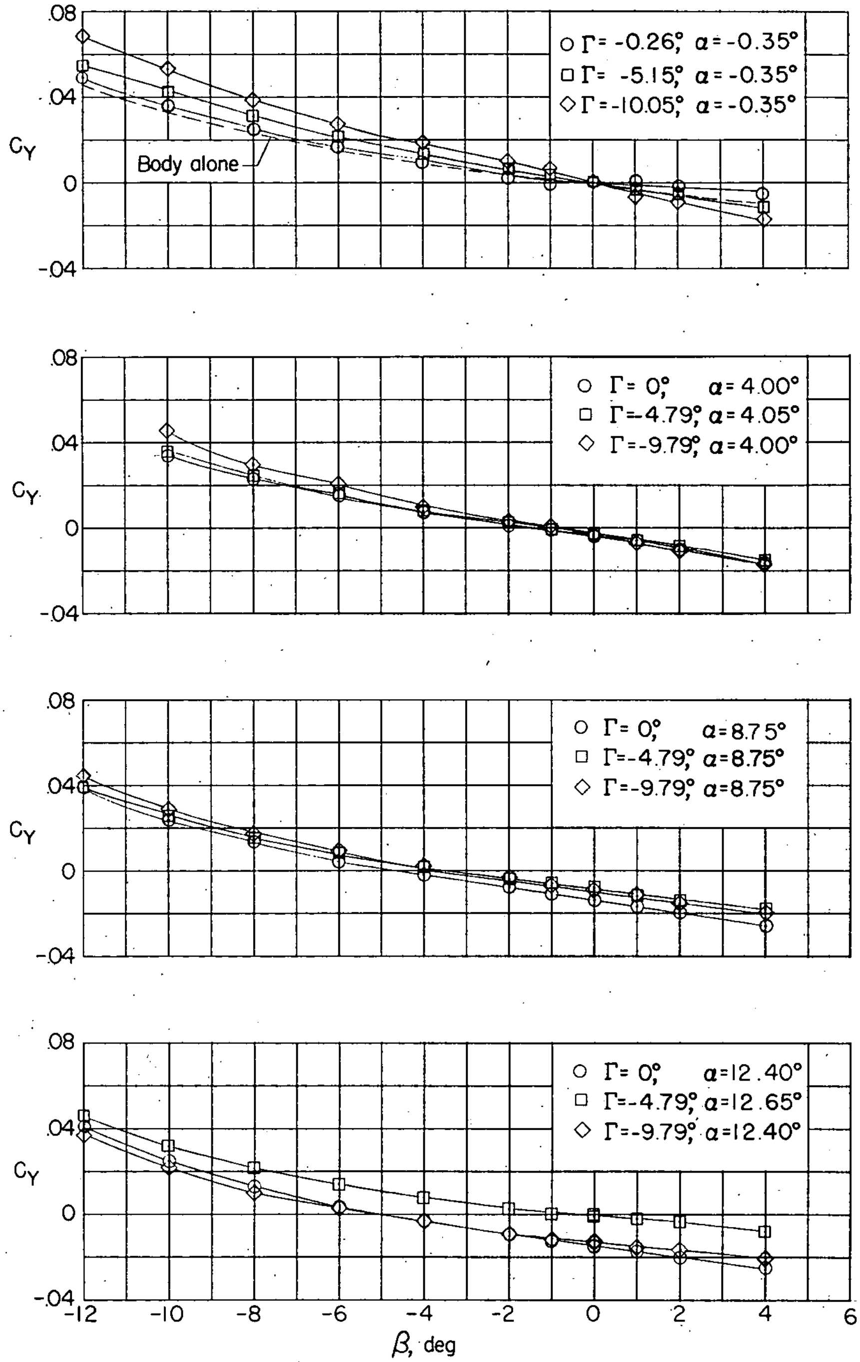

(c) Wing 2 at M = 1.62.

Figure 6.- Continued.

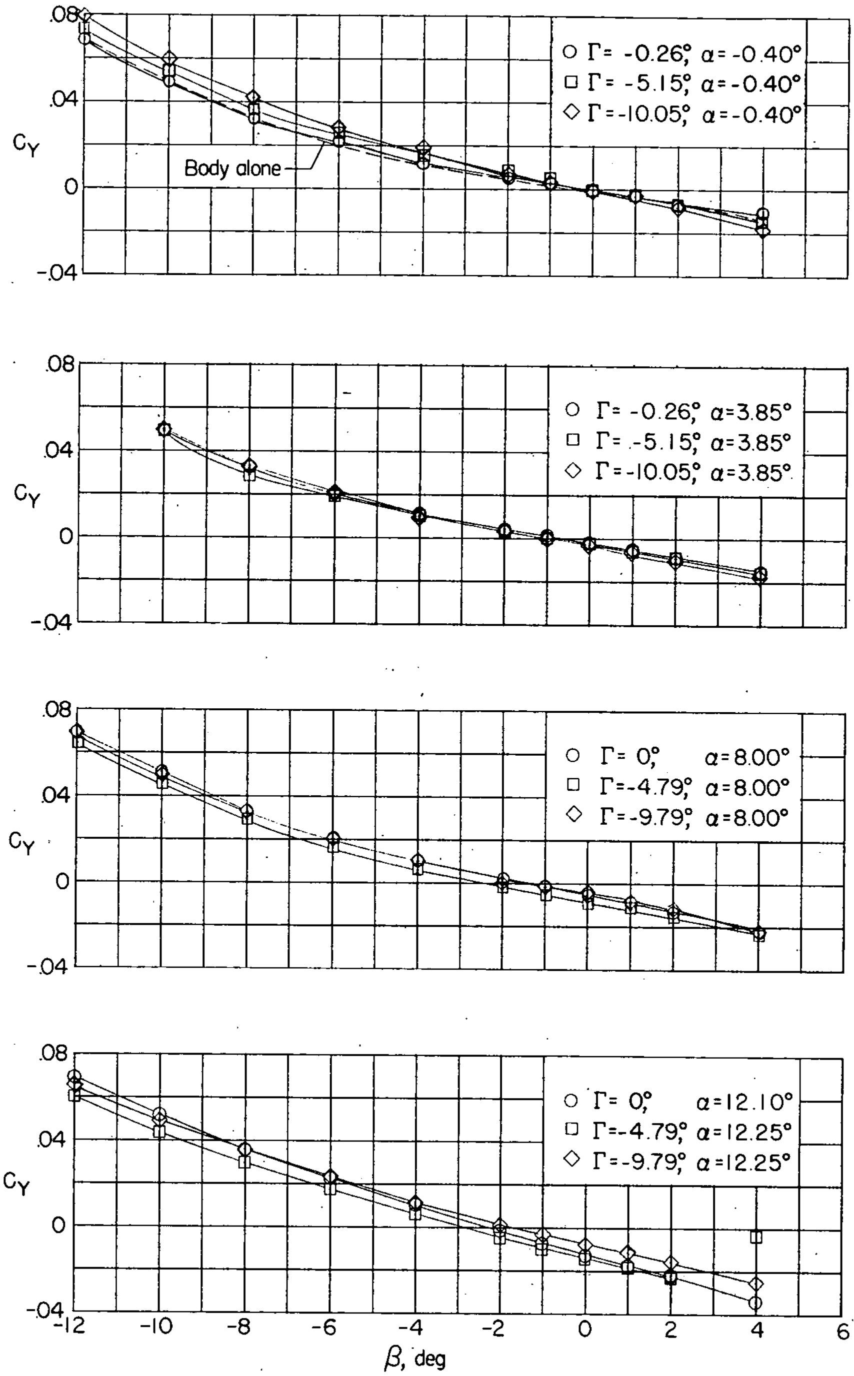

(d) Wing 2 at M = 2.62.

Figure 6.- Continued.

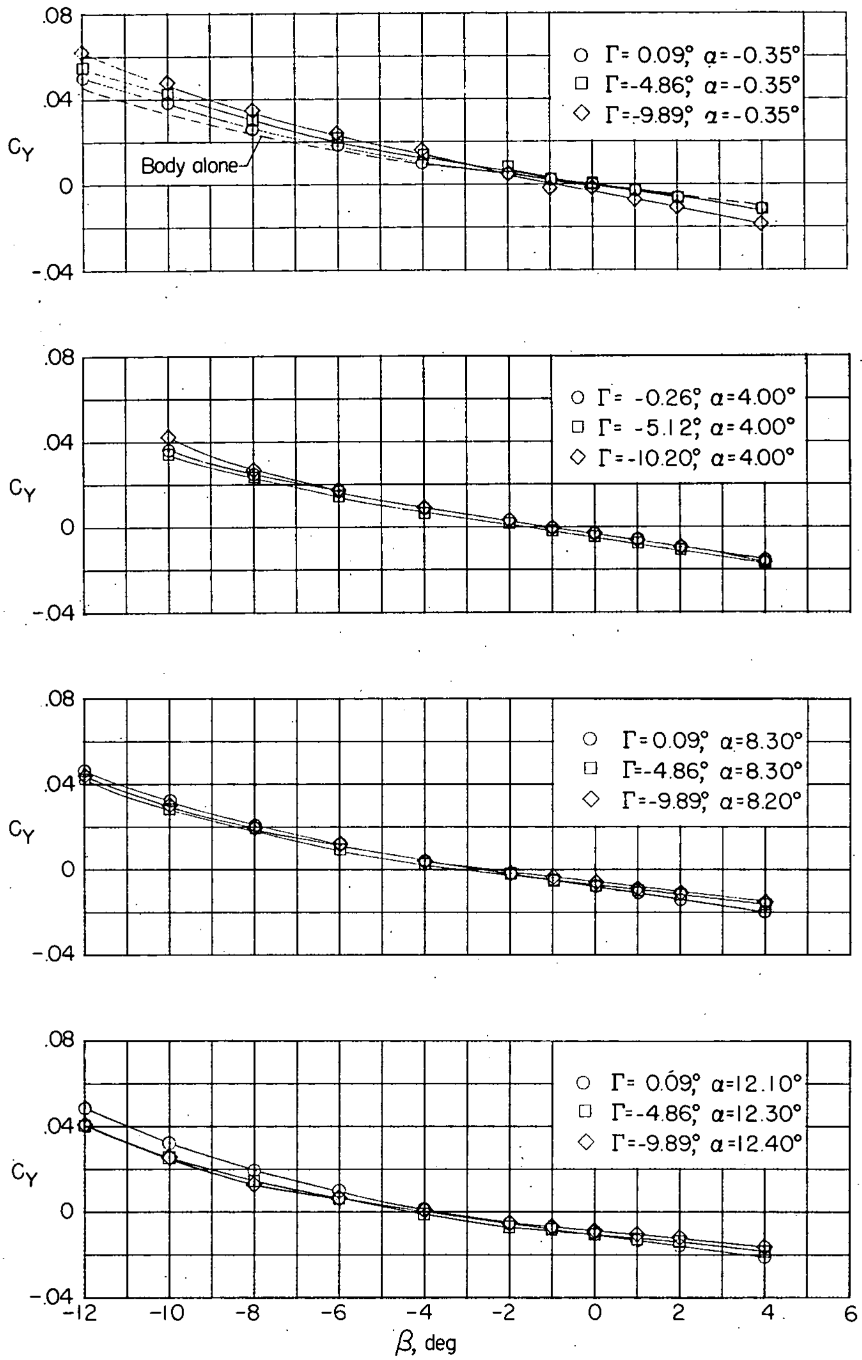

(e) Wing 3 at M = 1.62.

Figure 6.- Continued.

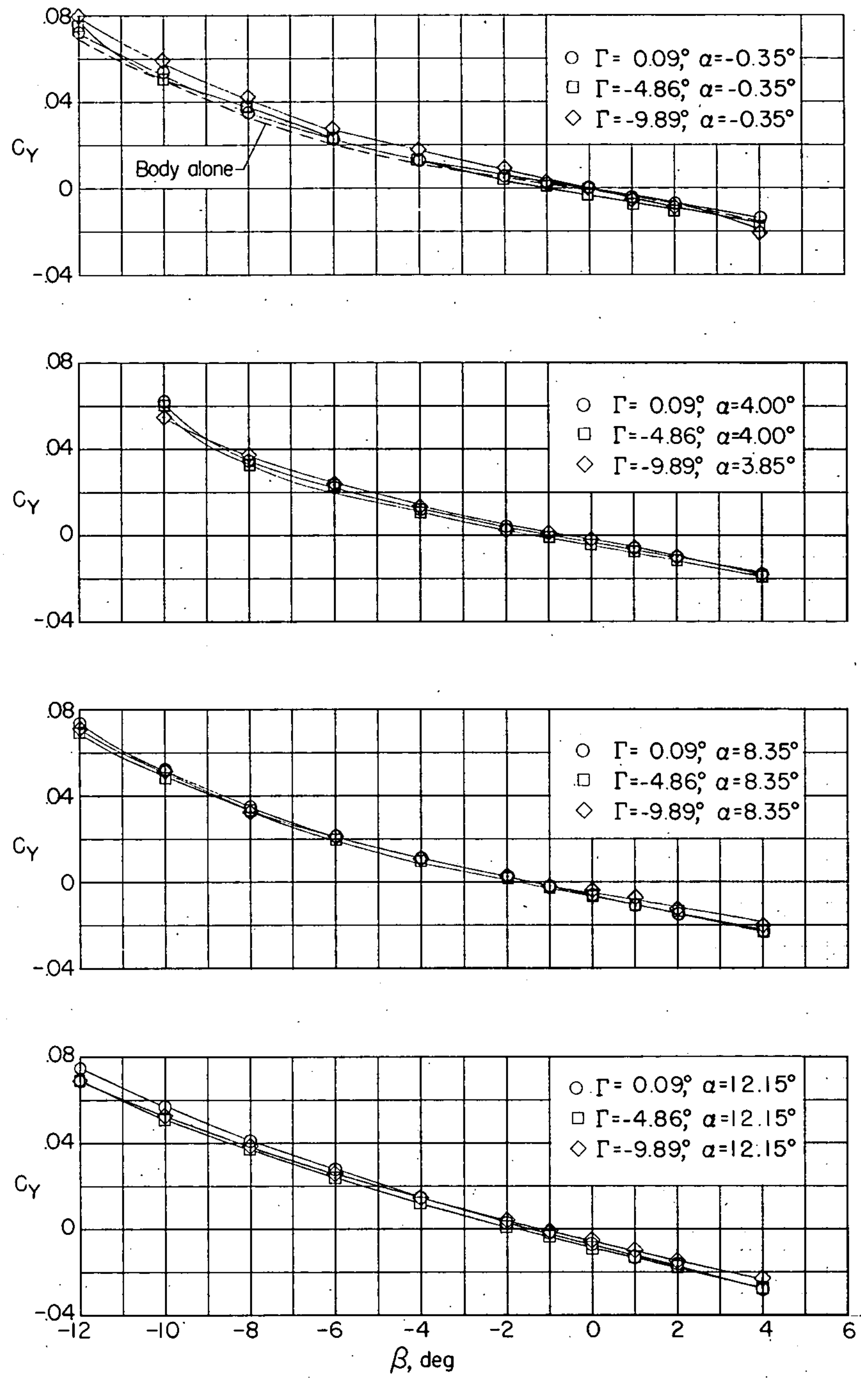

(f) Wing 3 at M = 2.62.

Figure 6.- Concluded.

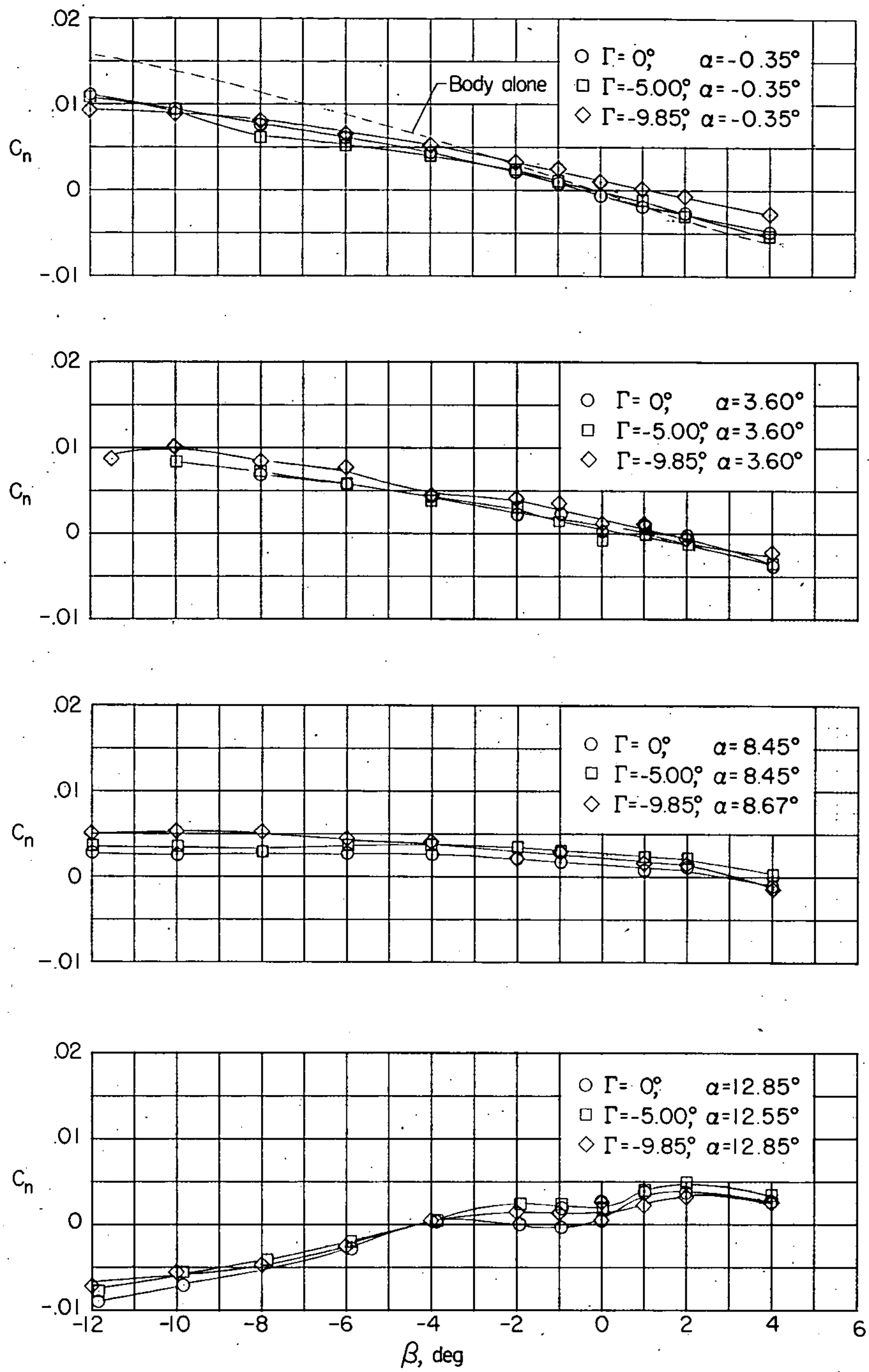

(a) Wing 1 at M = 1.62.

Figure 7.- Yawing-moment characteristics of wing-body combinations. (Wind-axis system.)

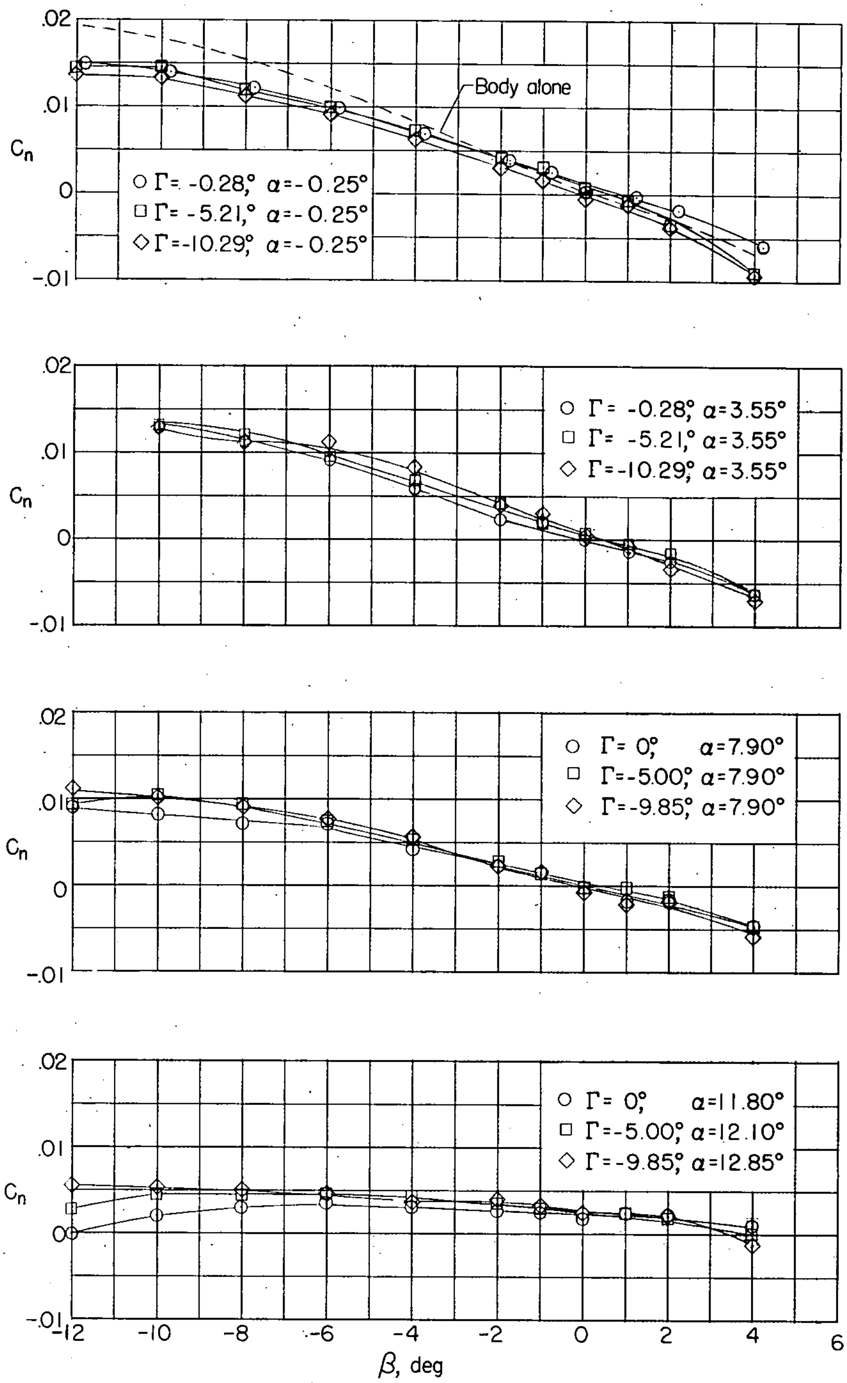

(b) Wing 1 at M = 2.62.

Figure 7.- Continued.

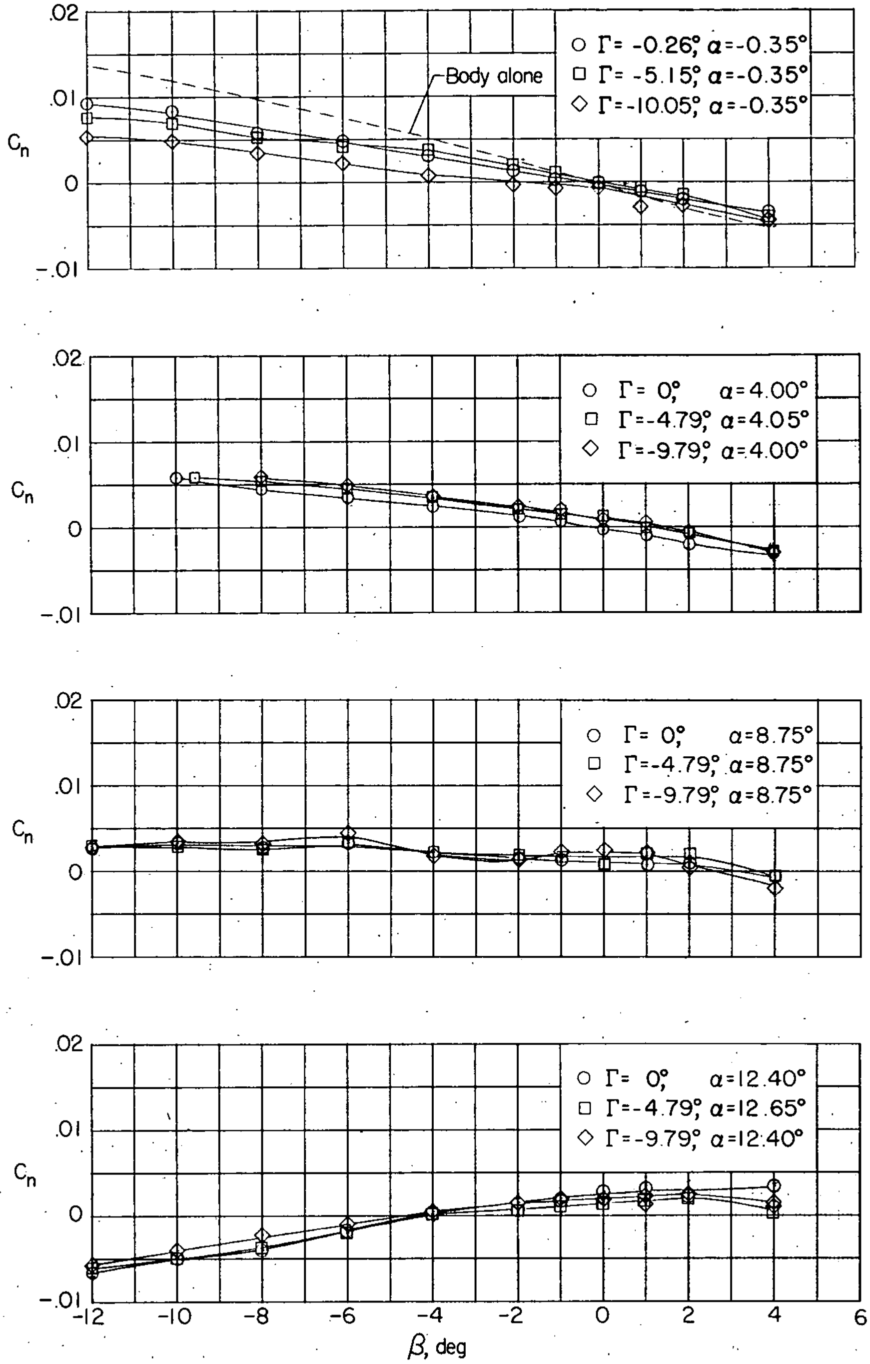

(c) Wing 2 at M = 1.62.

Figure 7.- Continued.

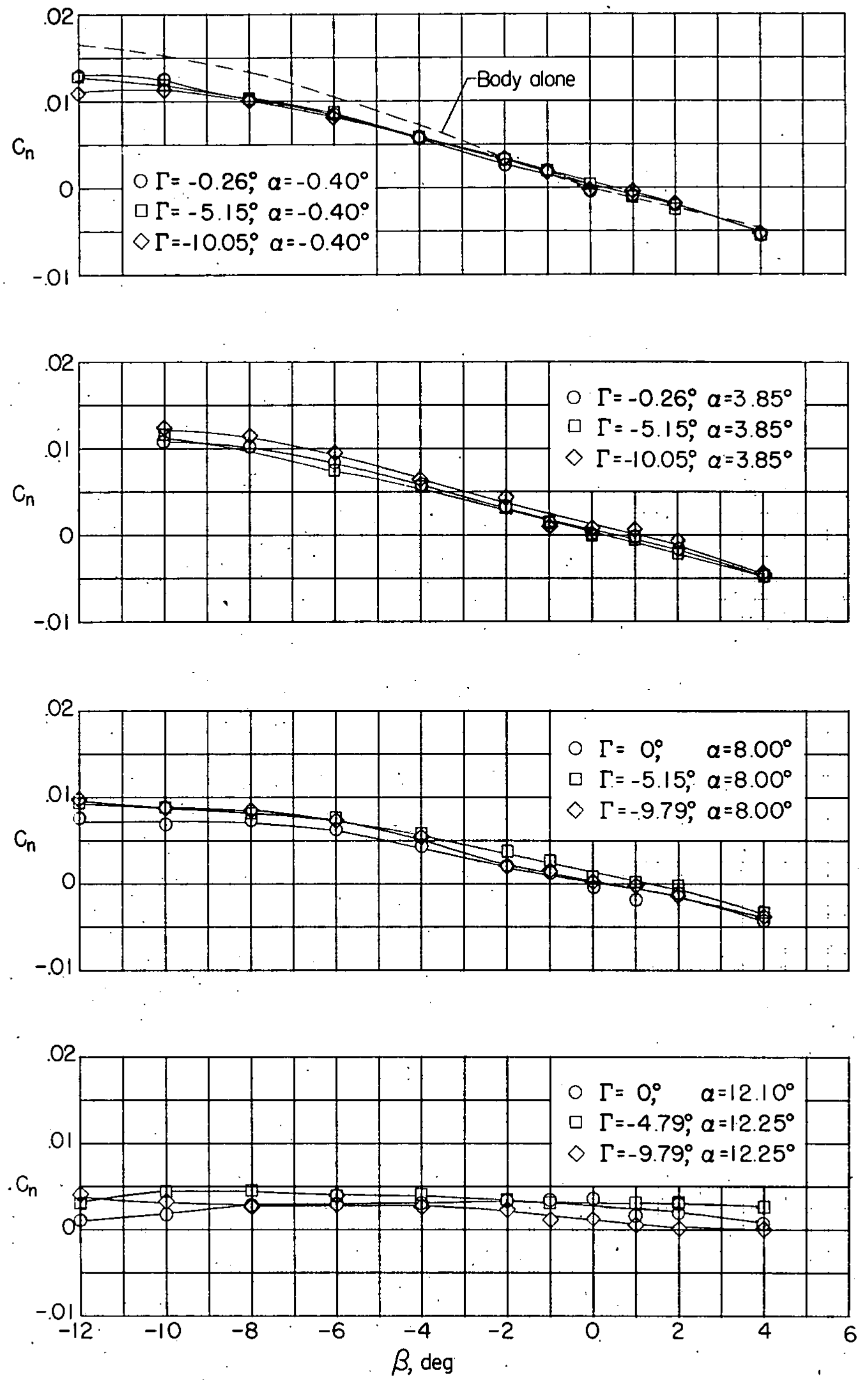

(d) Wing 2 at M = 2.62.

Figure 7.- Continued.

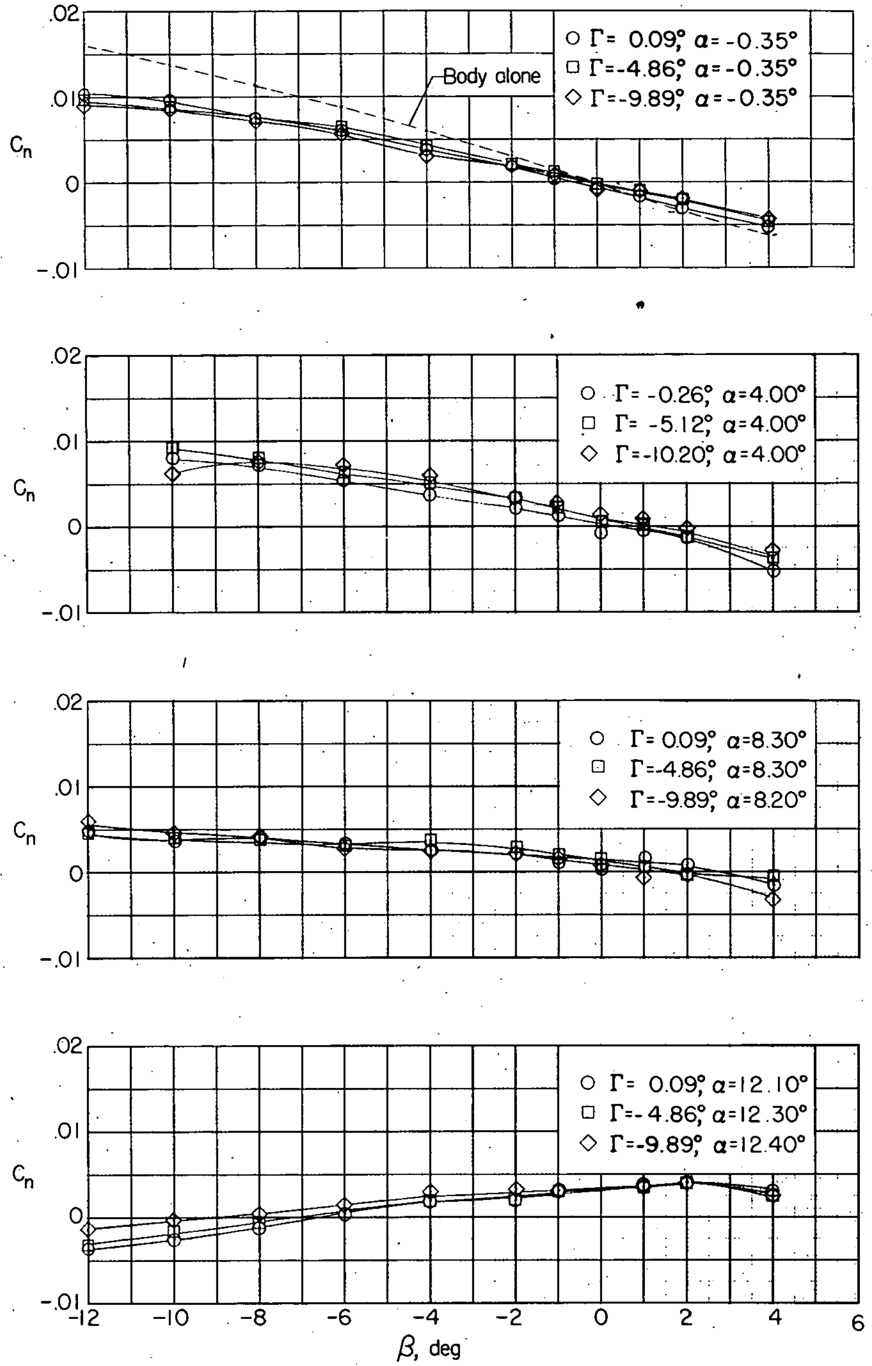

(e) Wing 3 at M = 1.62.

Figure 7.- Continued.

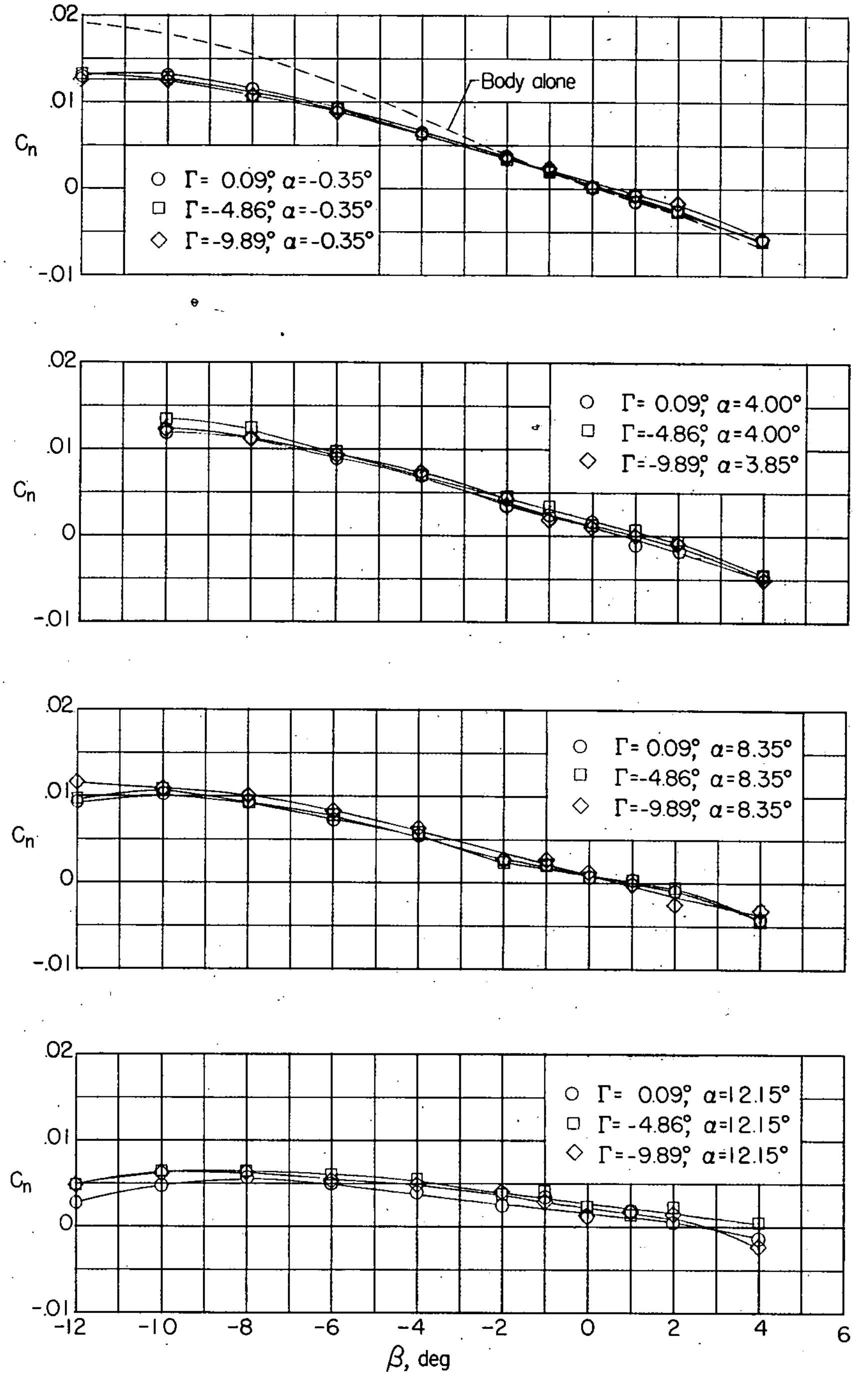

(f) Wing 3 at M = 2.62.

Figure 7.- Concluded.

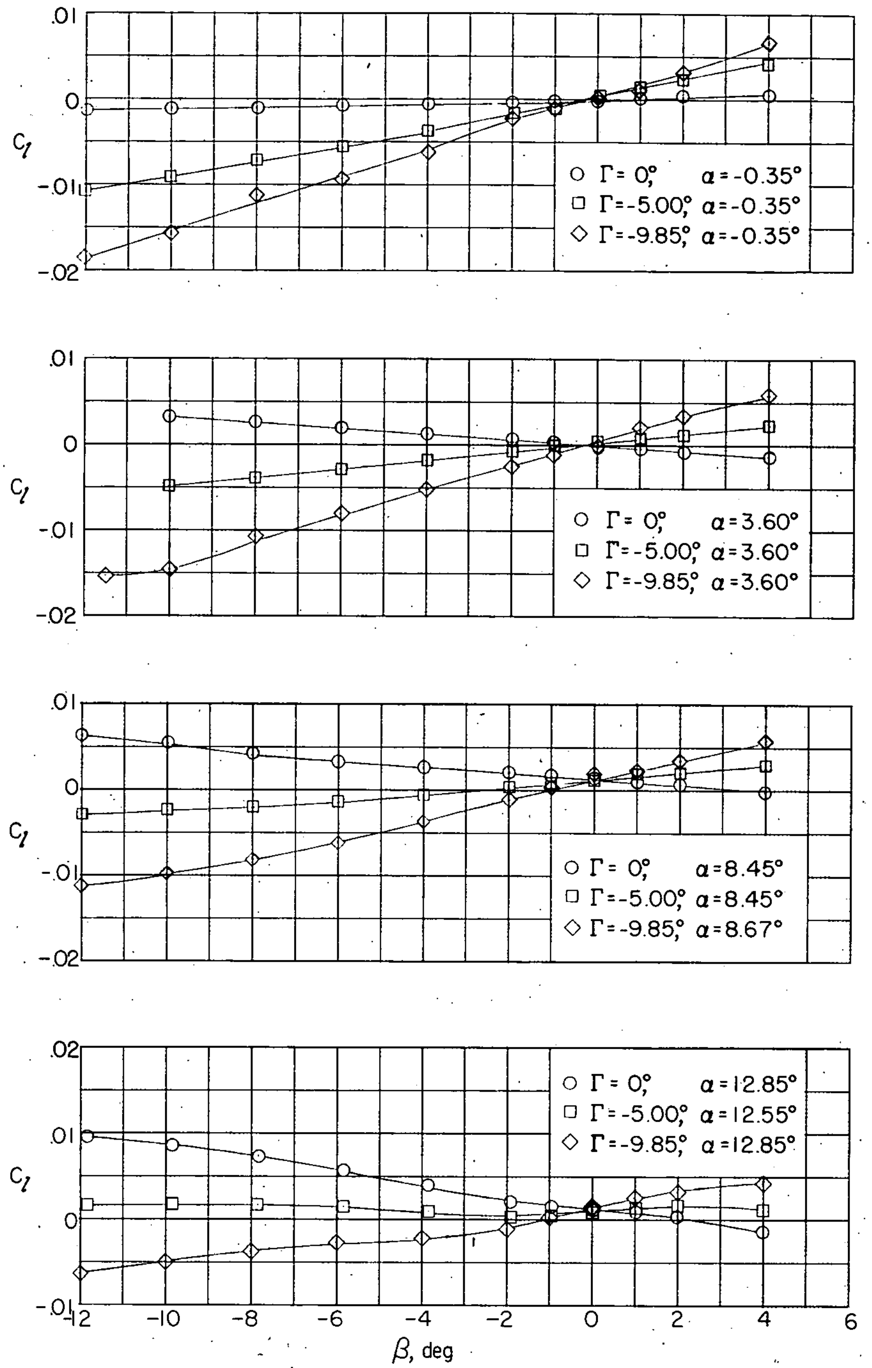

(a) Wing 1 at M = 1.62.

Figure 8.- Rolling-moment characteristics of wing-body combinations. (Body-axis system.)

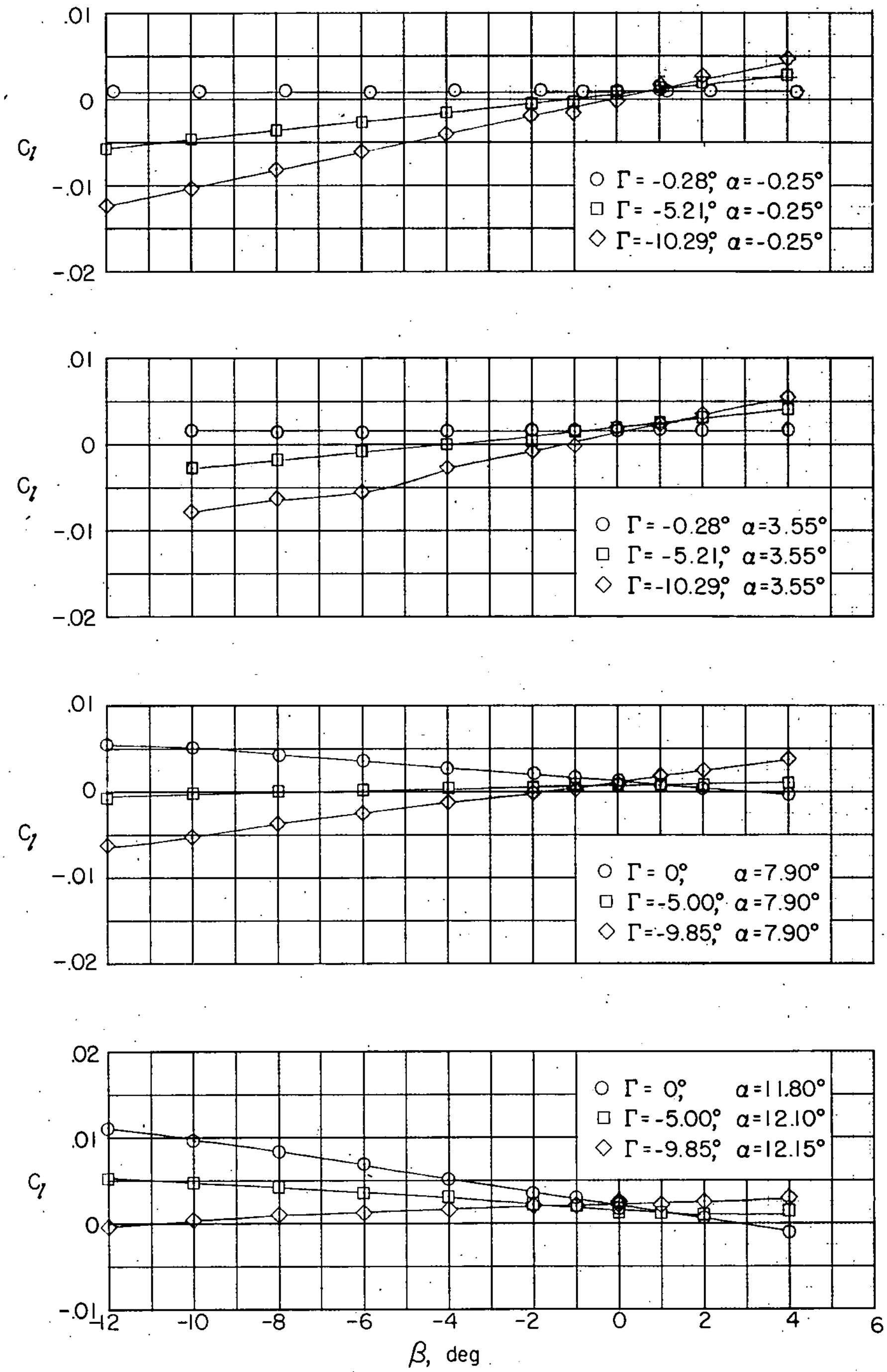

(b) Wing 1 at M = 2.62.

Figure 8.- Continued.

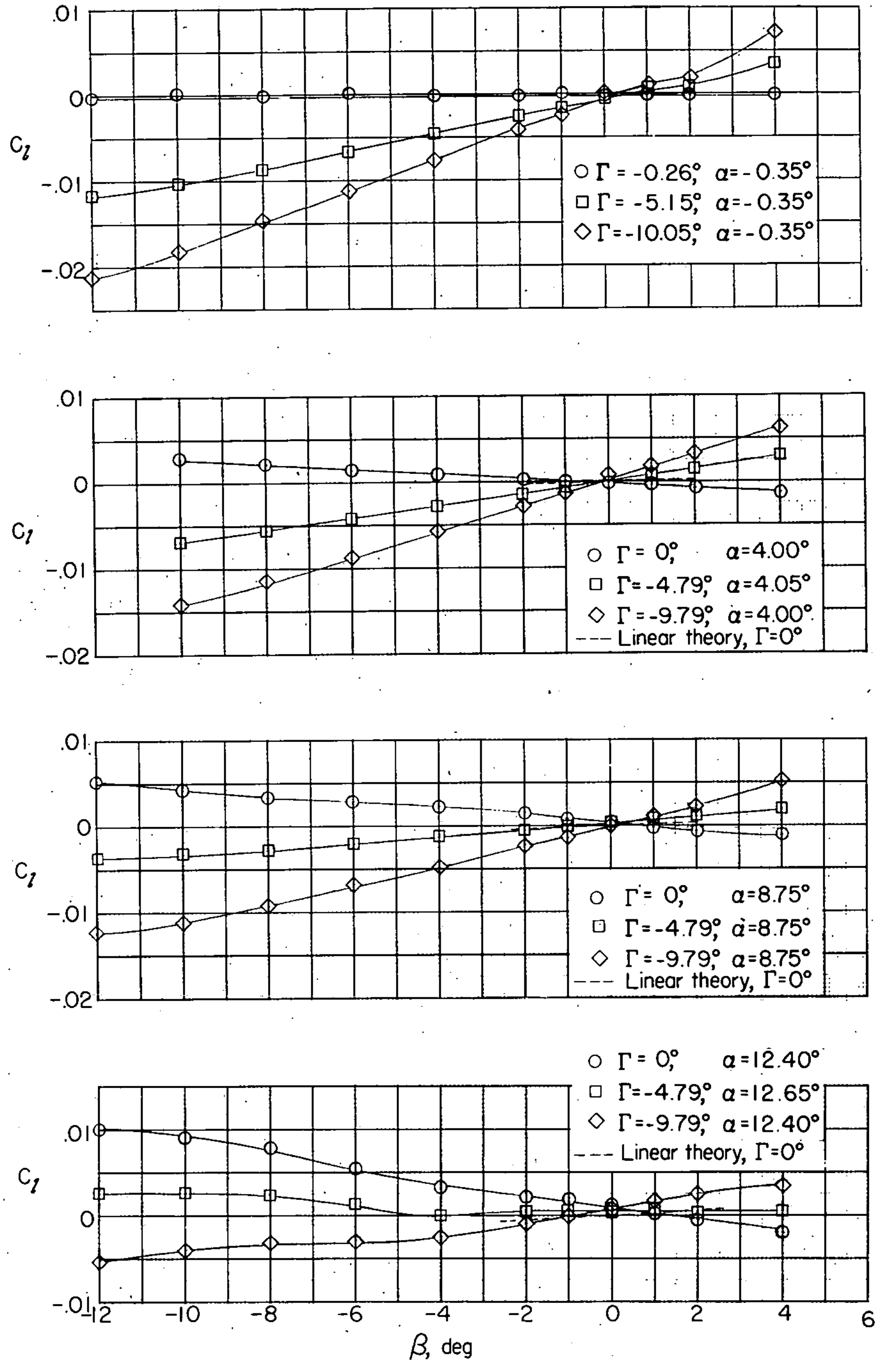

(c) Wing 2 at M = 1.62.

Figure 8.- Continued.

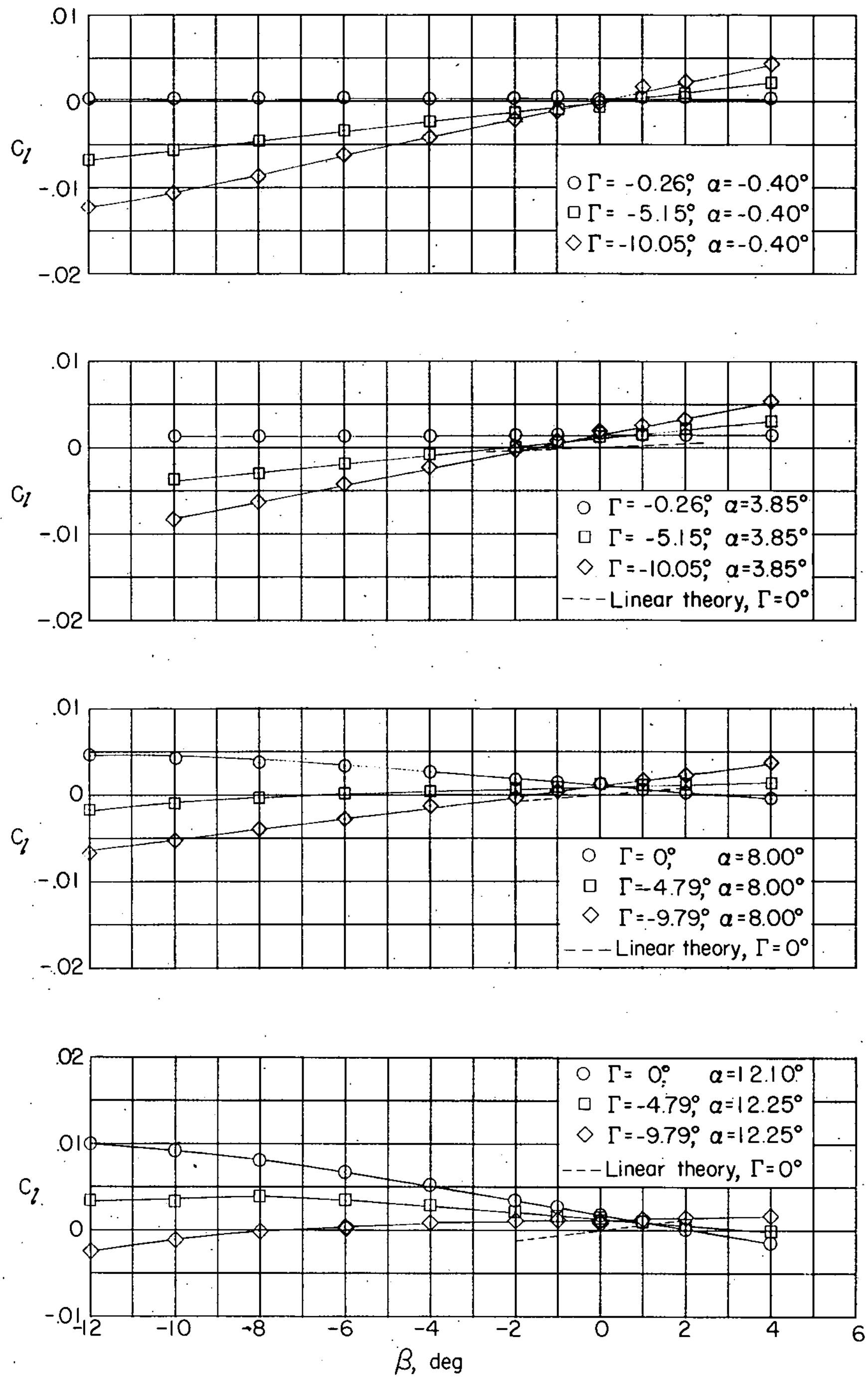

(d) Wing 2 at M = 2.62.

Figure 8.- Continued.

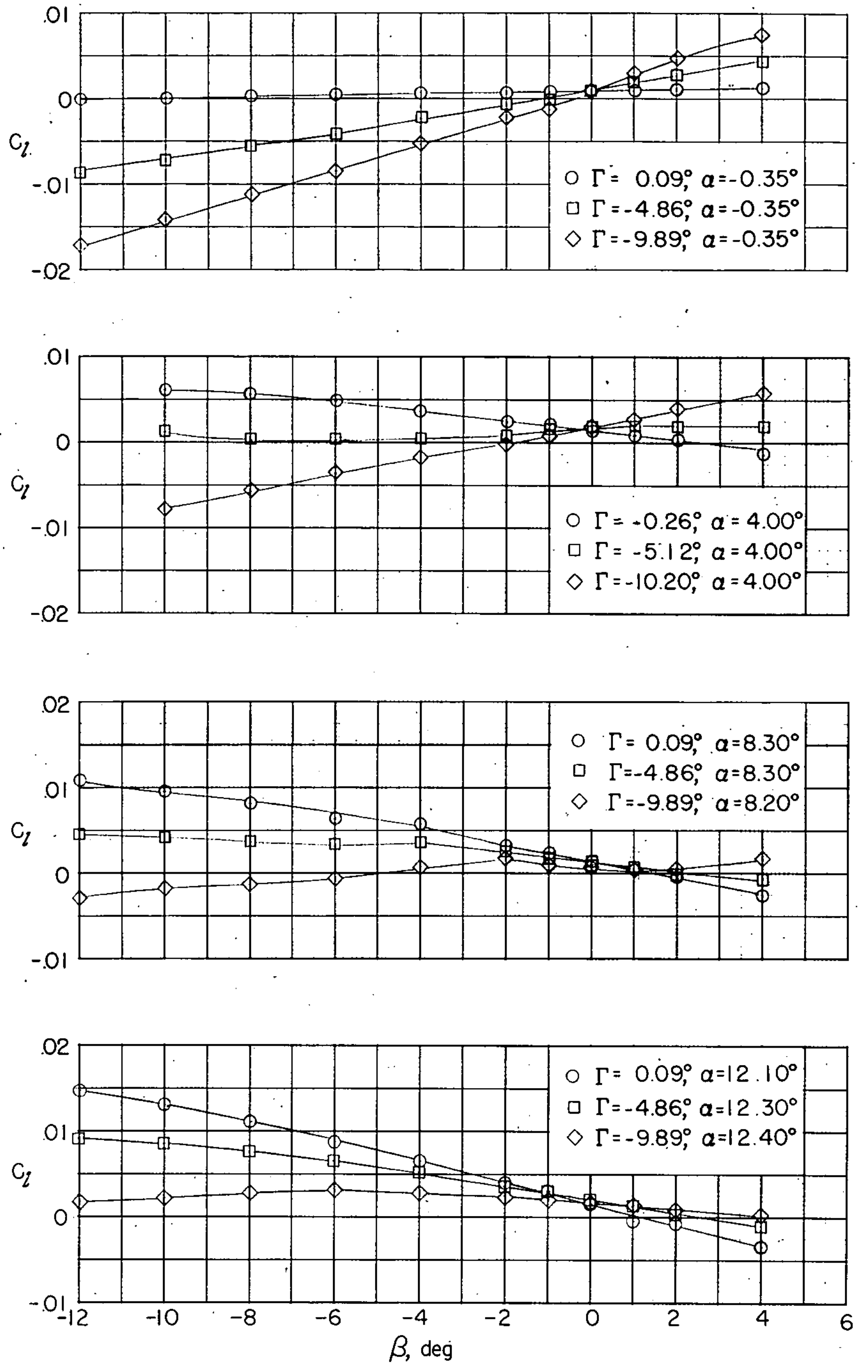

(e) Wing 3 at M = 1.62.

Figure 8.- Continued.

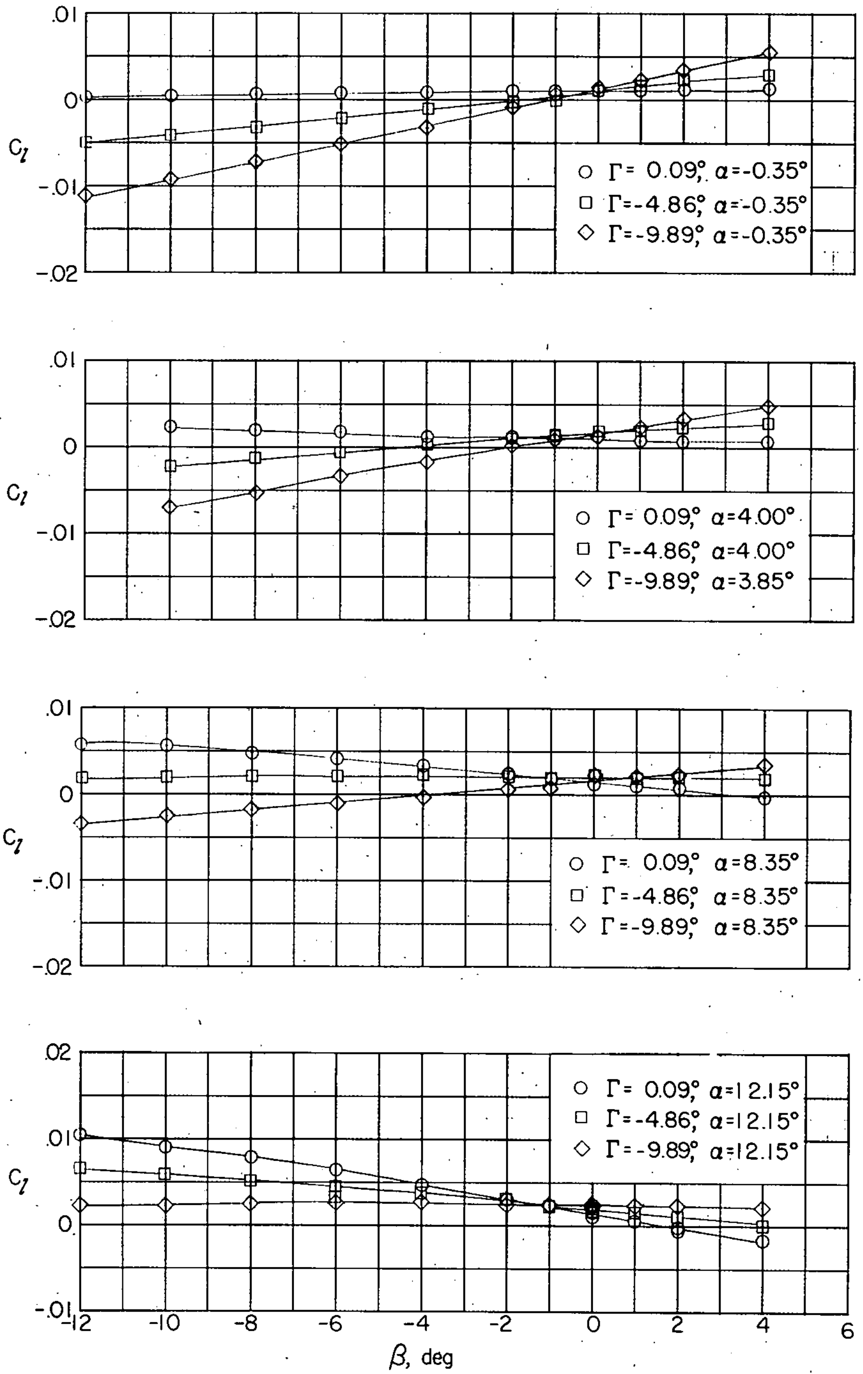

(f) Wing 3 at M = 2.62.

Figure 8.- Concluded.

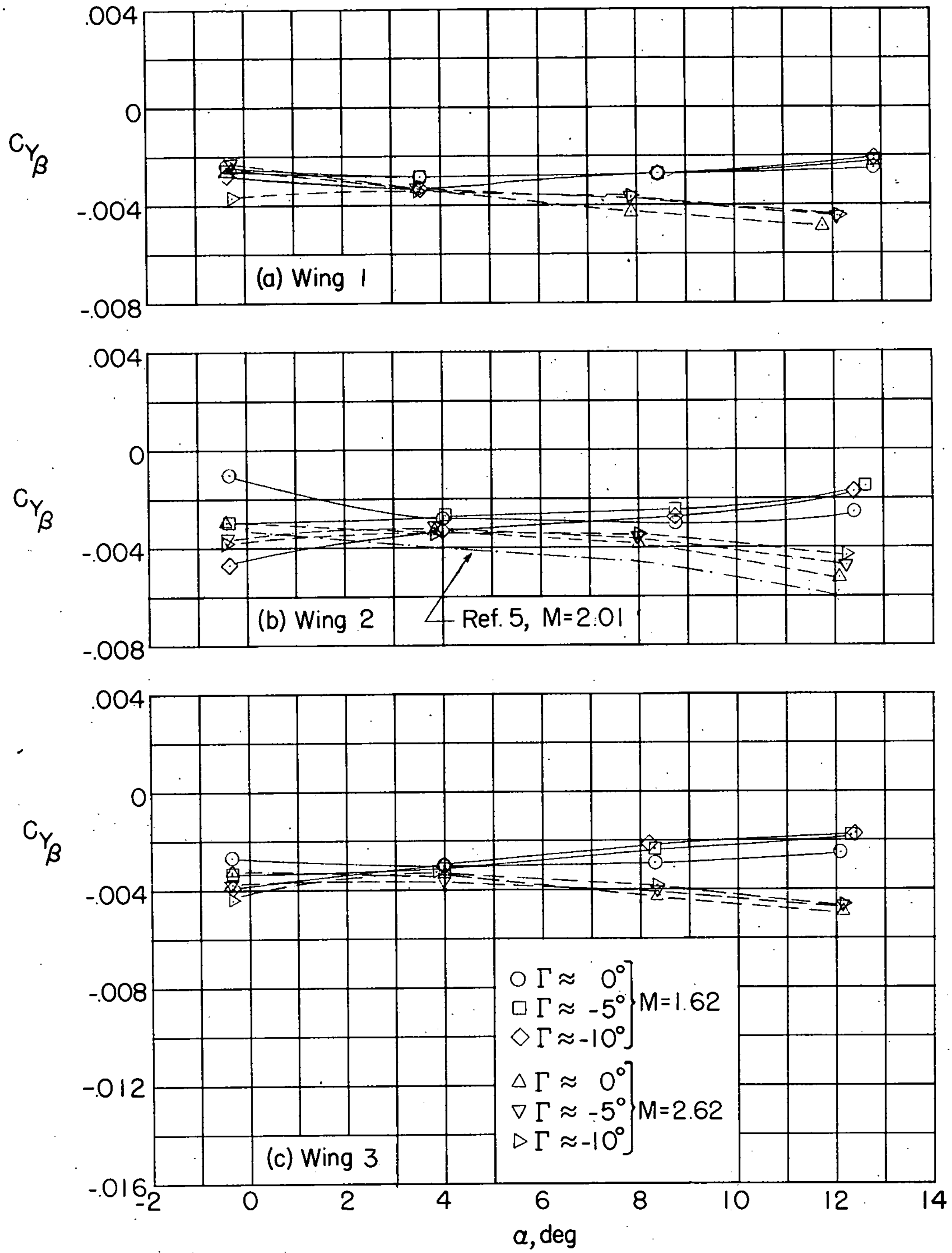

Figure 9.- Variation of C_{Y_β} with α for the wing-body combinations. (Slopes were taken over range of β of $\pm 2^{\circ}$.)

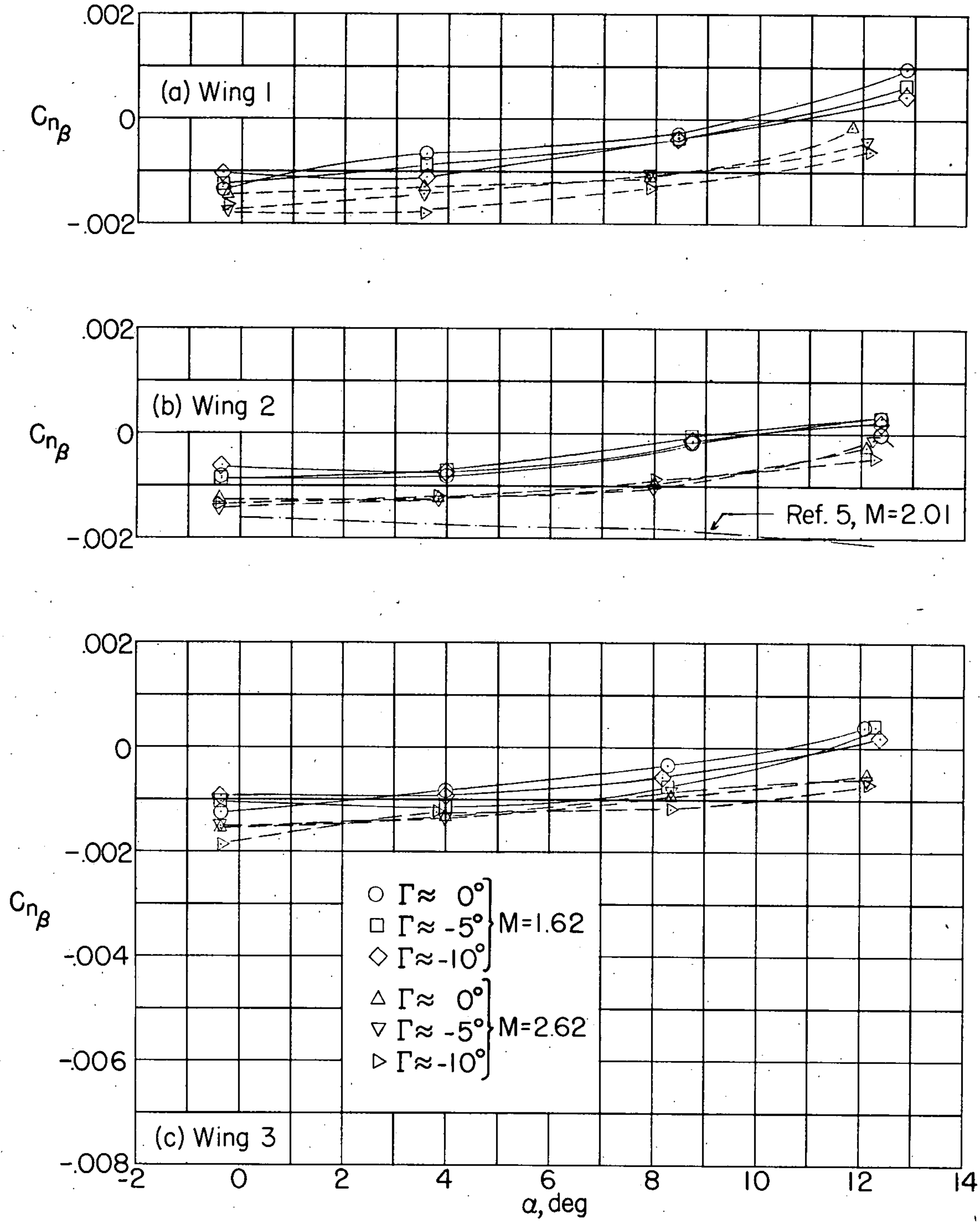

Figure 10.- Variation of C_{n_β} with α for the wing-body combinations. Flagged symbol indicates no transition. (Slopes were taken over range of β of $\pm 2^{\circ}$.)

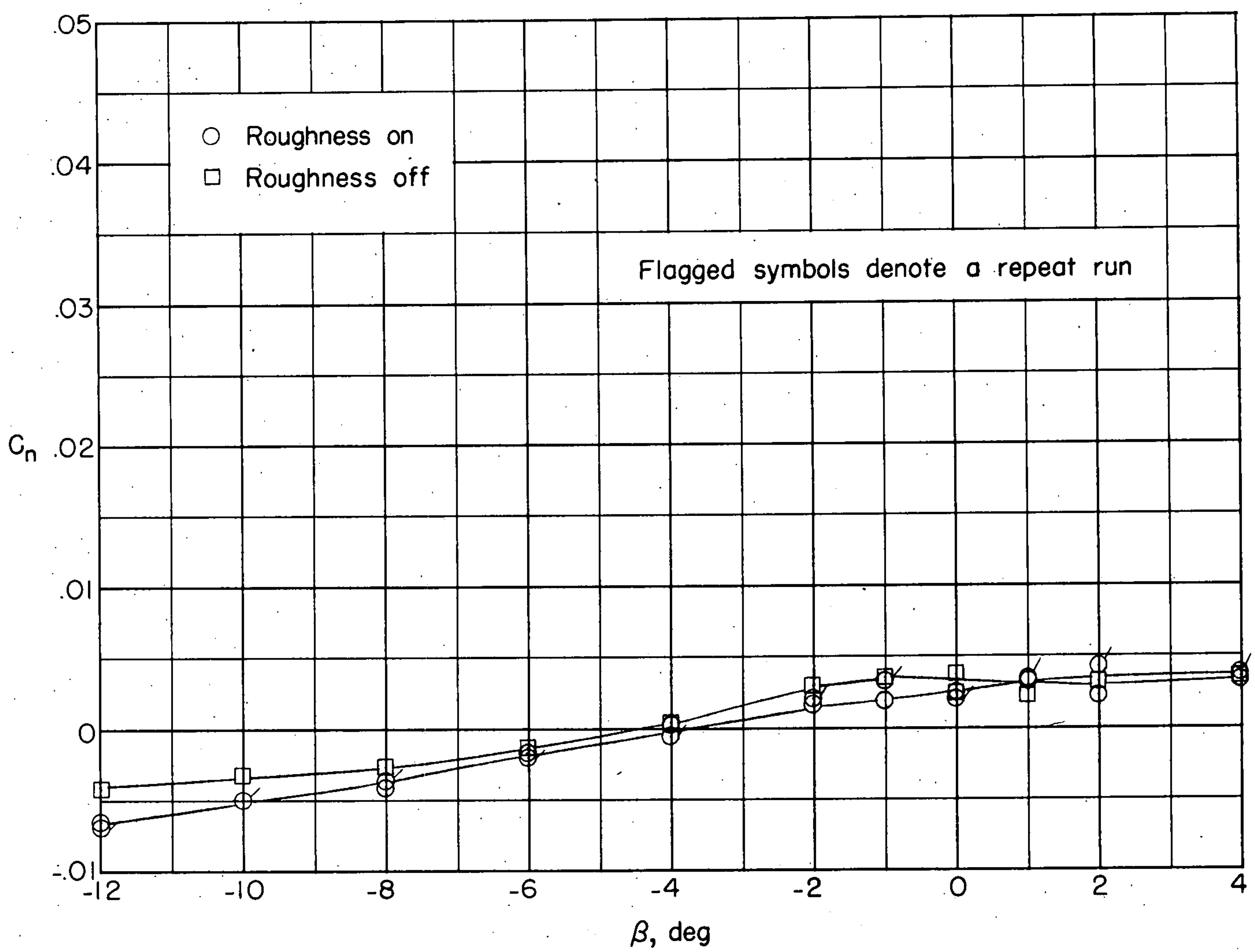

Figure 11.- Variation of C_n with β for wing 2 at $M = 1.62$, showing effect of roughness strips. $\alpha = 12.40^{\circ}$; $\Gamma = 0^{\circ}$.

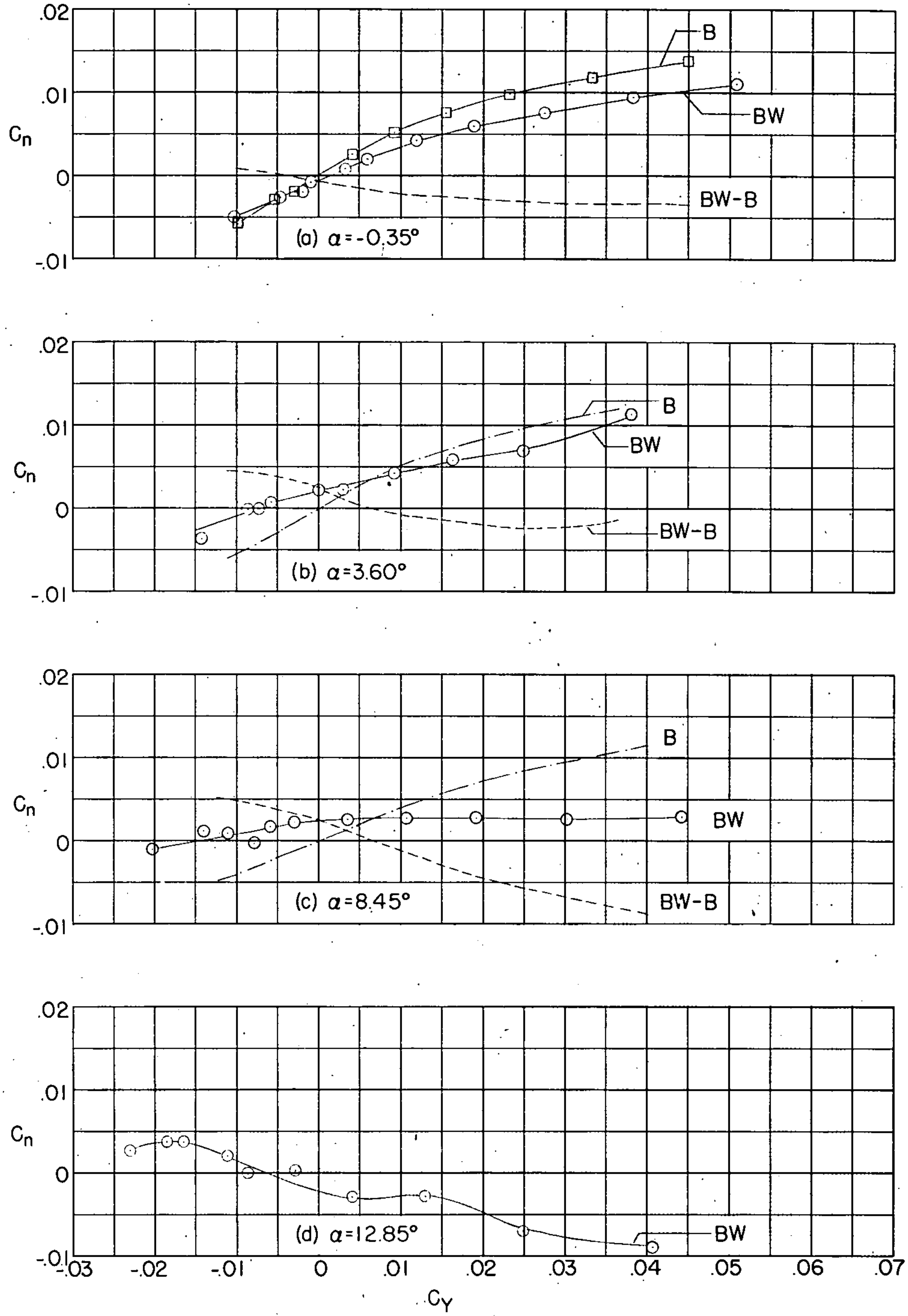

Figure 12.- Variation of C_n with C_Y for individual and combined components of the wing-body combinations. Wing 1 at $M = 1.62$.

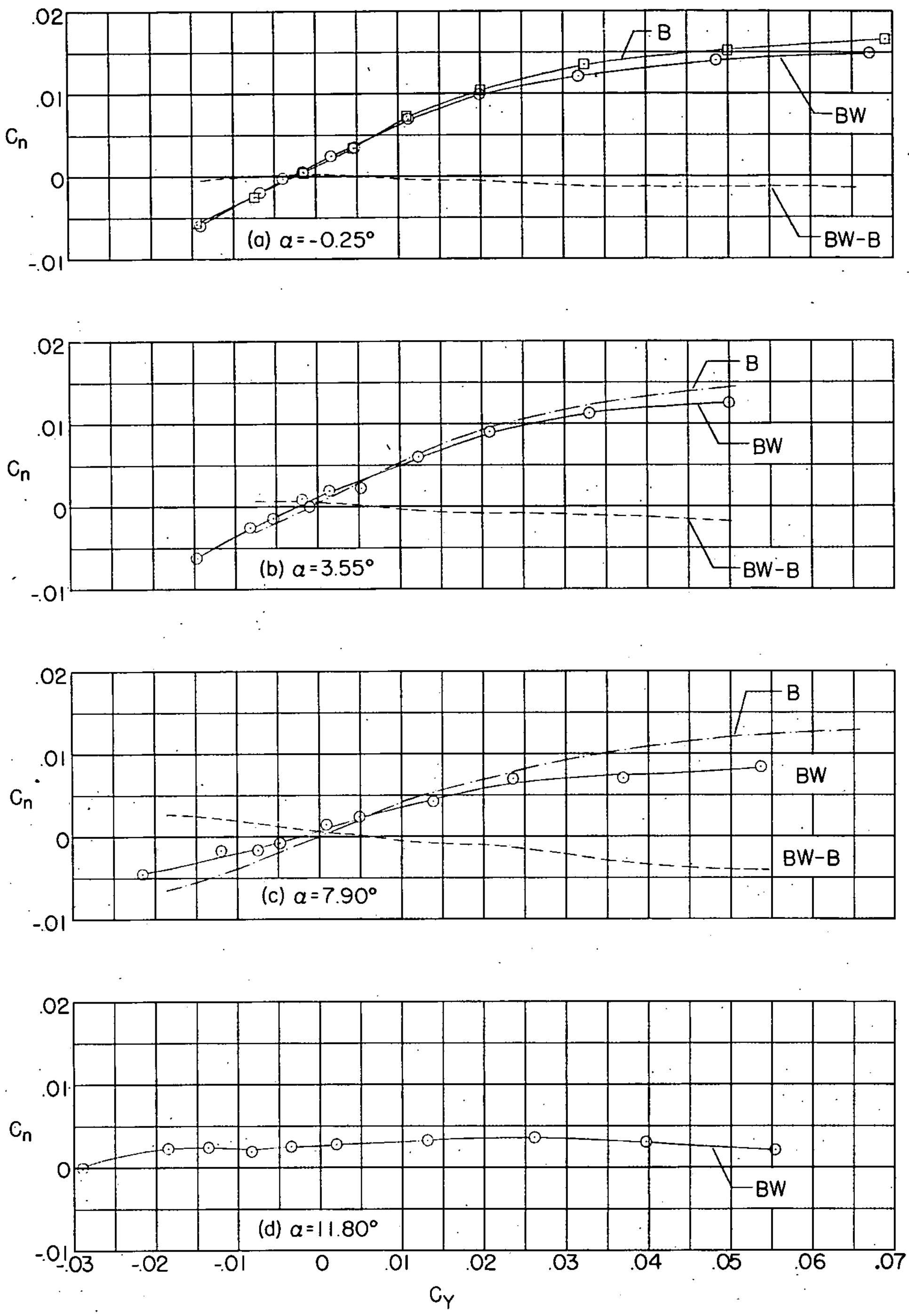

Figure 13.- Variation of C_n with C_Y for individual and combined components of the wing-body combinations. Wing 1 at $M = 2.62$.

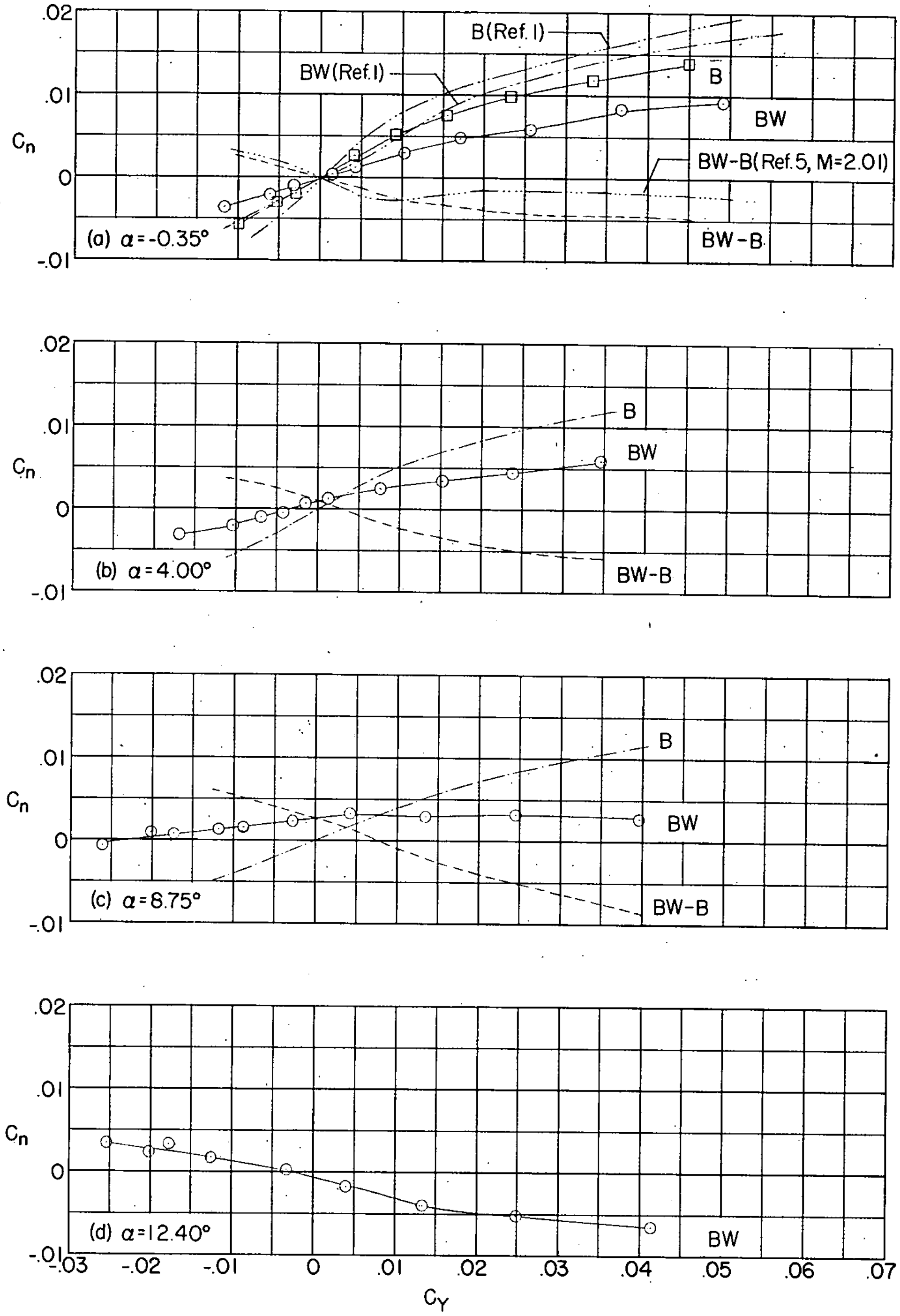

Figure 14.- Variation of C_n with C_Y for individual and combined components of the wing-body combinations. Wing 2 at $M = 1.62$.

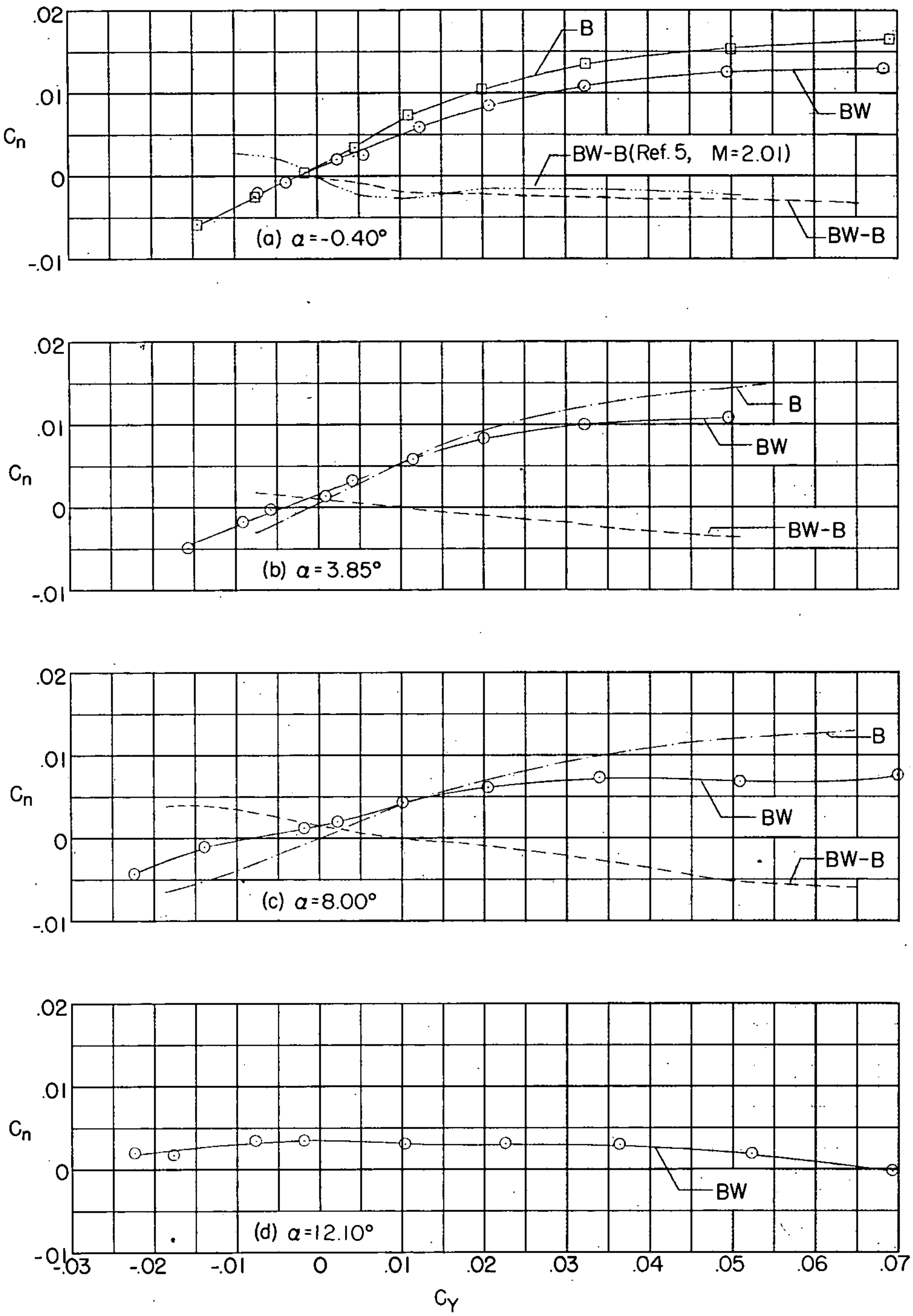

Figure 15.- Variation of C_n with C_Y for individual and combined components of the wing-body combinations. Wing 2 at M = 2.62.

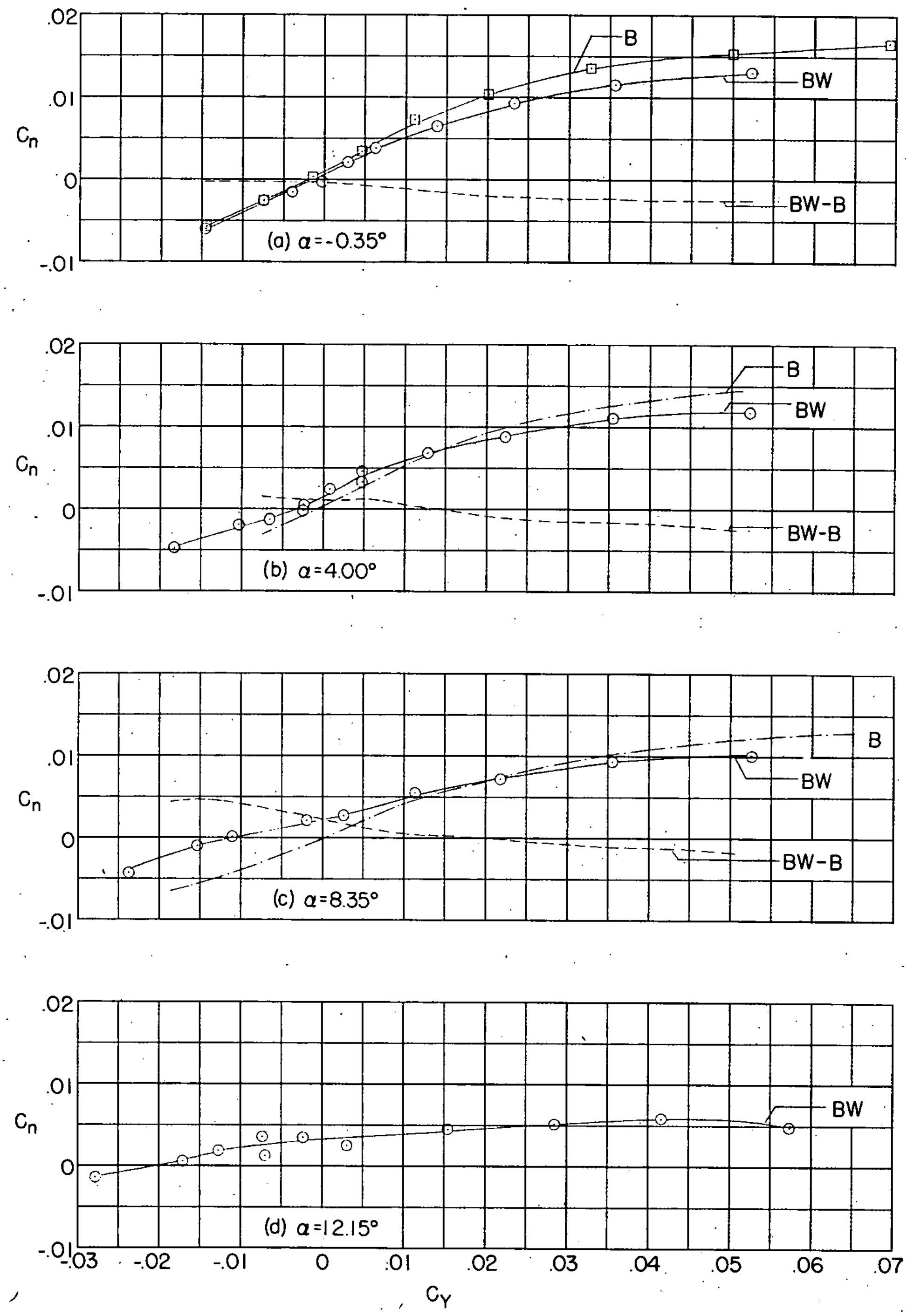

Figure 16.- Variation of C_n with C_Y for individual and combined components of the wing-body combinations. Wing 3 at M = 2.62.

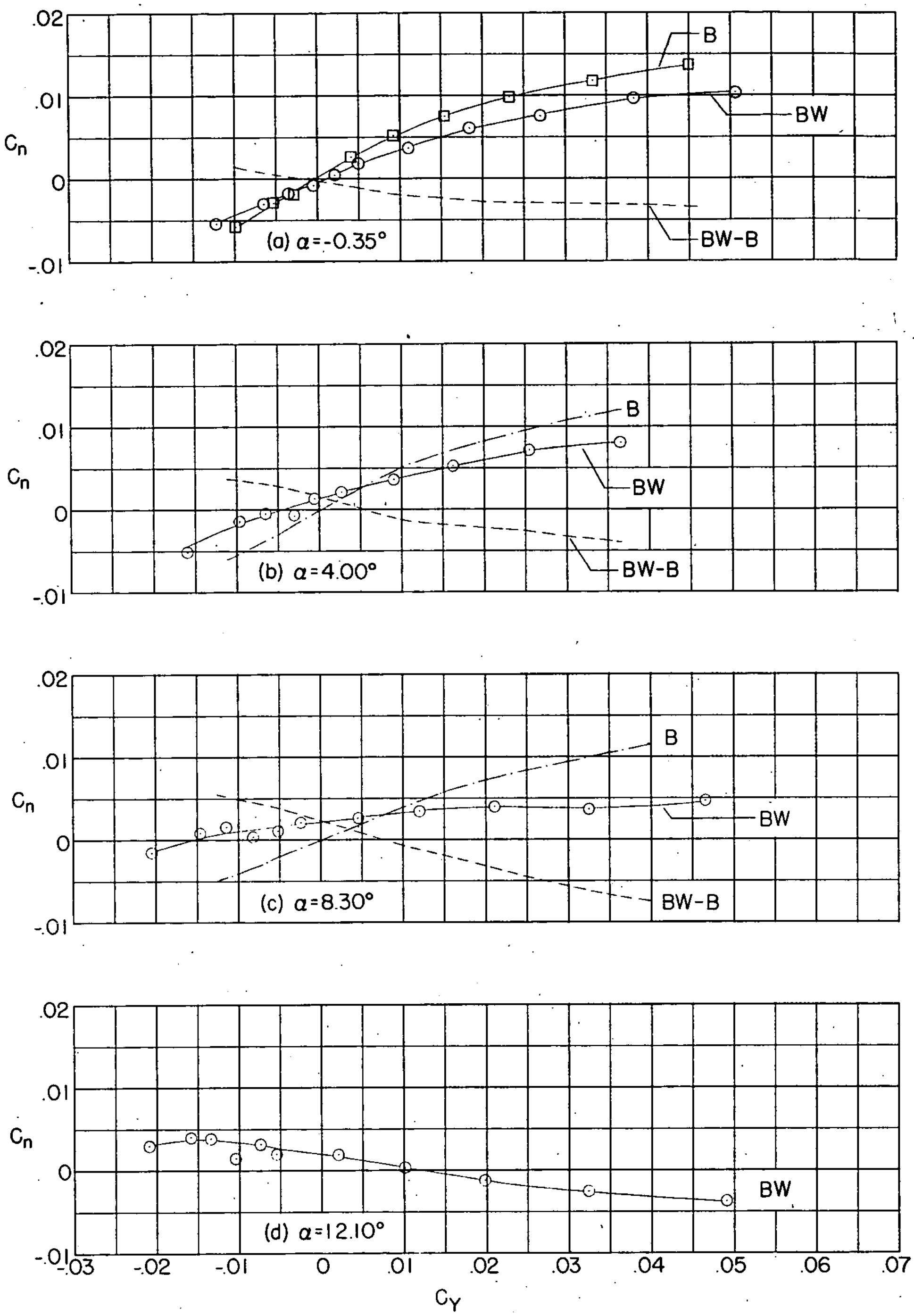

Figure 17.- Variation of C_n with C_Y for individual and combined components of the wing-body combinations. Wing 3 at $M = 1.62$.

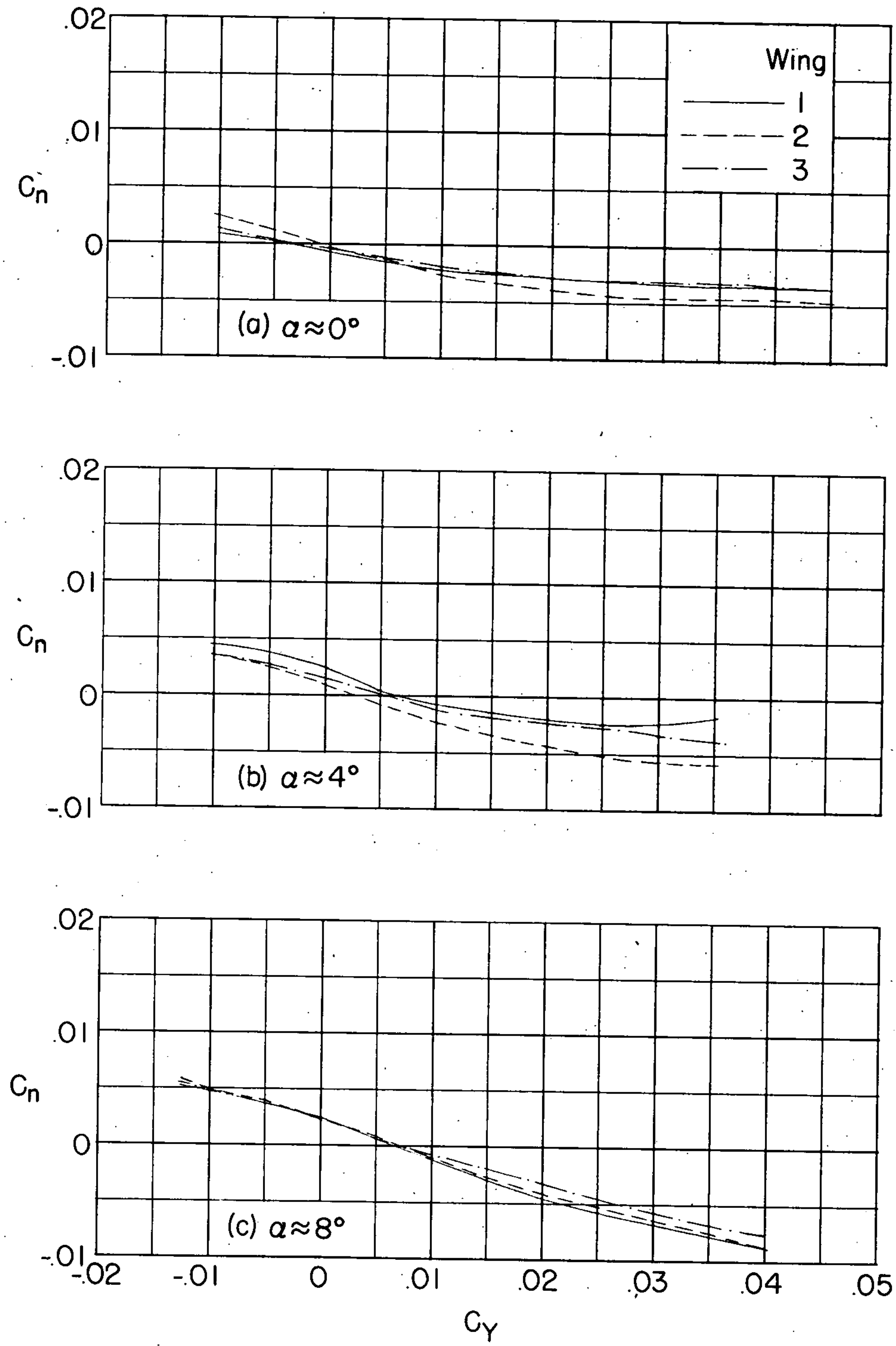

Figure 18.- Summary plots illustrating effect of wing plan form on variation of C_n with C_Y at $M = 1.62$.

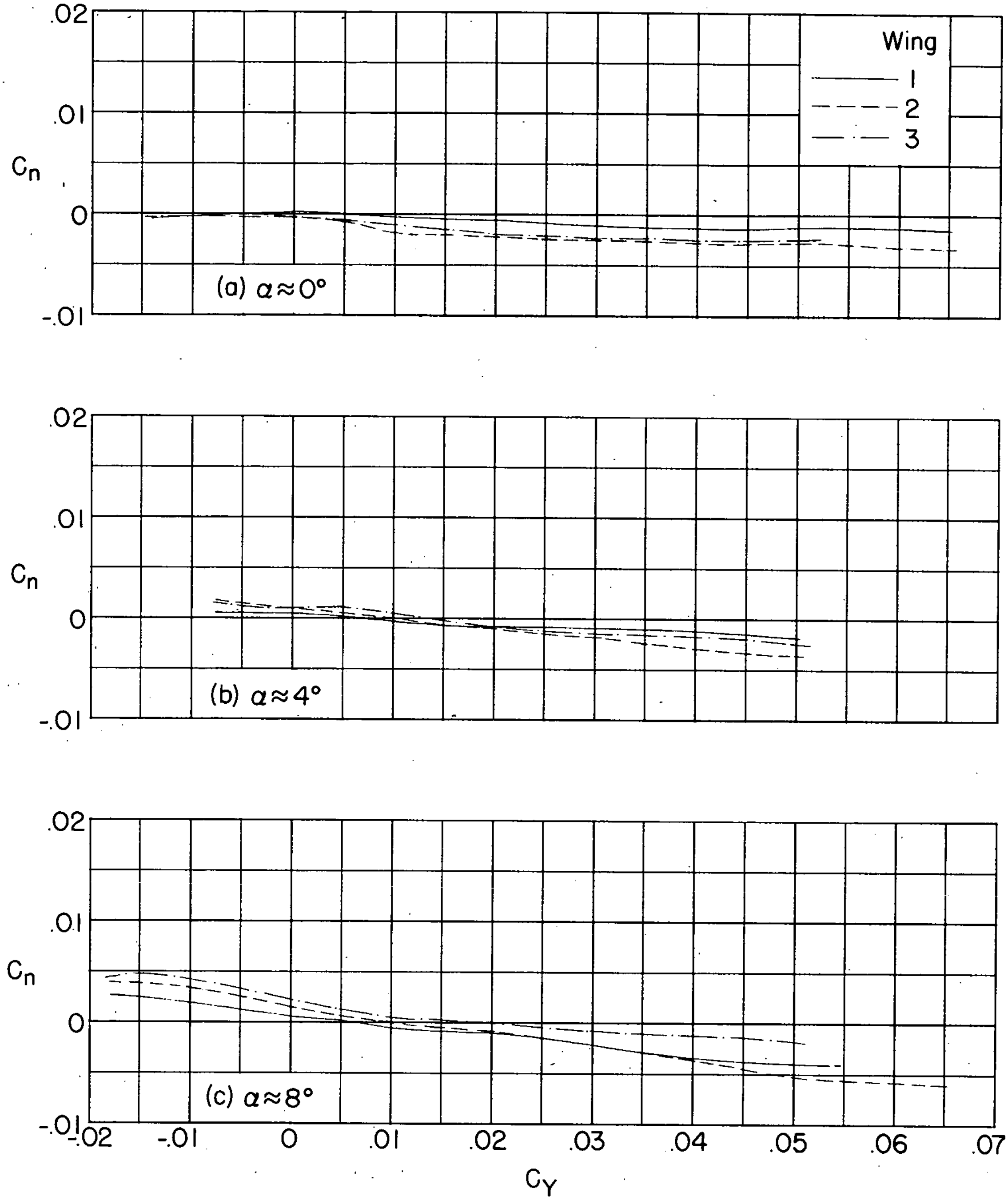

Figure 19.- Summary plots illustrating effect of wing plan form on variation of C_n with C_Y at $M = 2.62$.

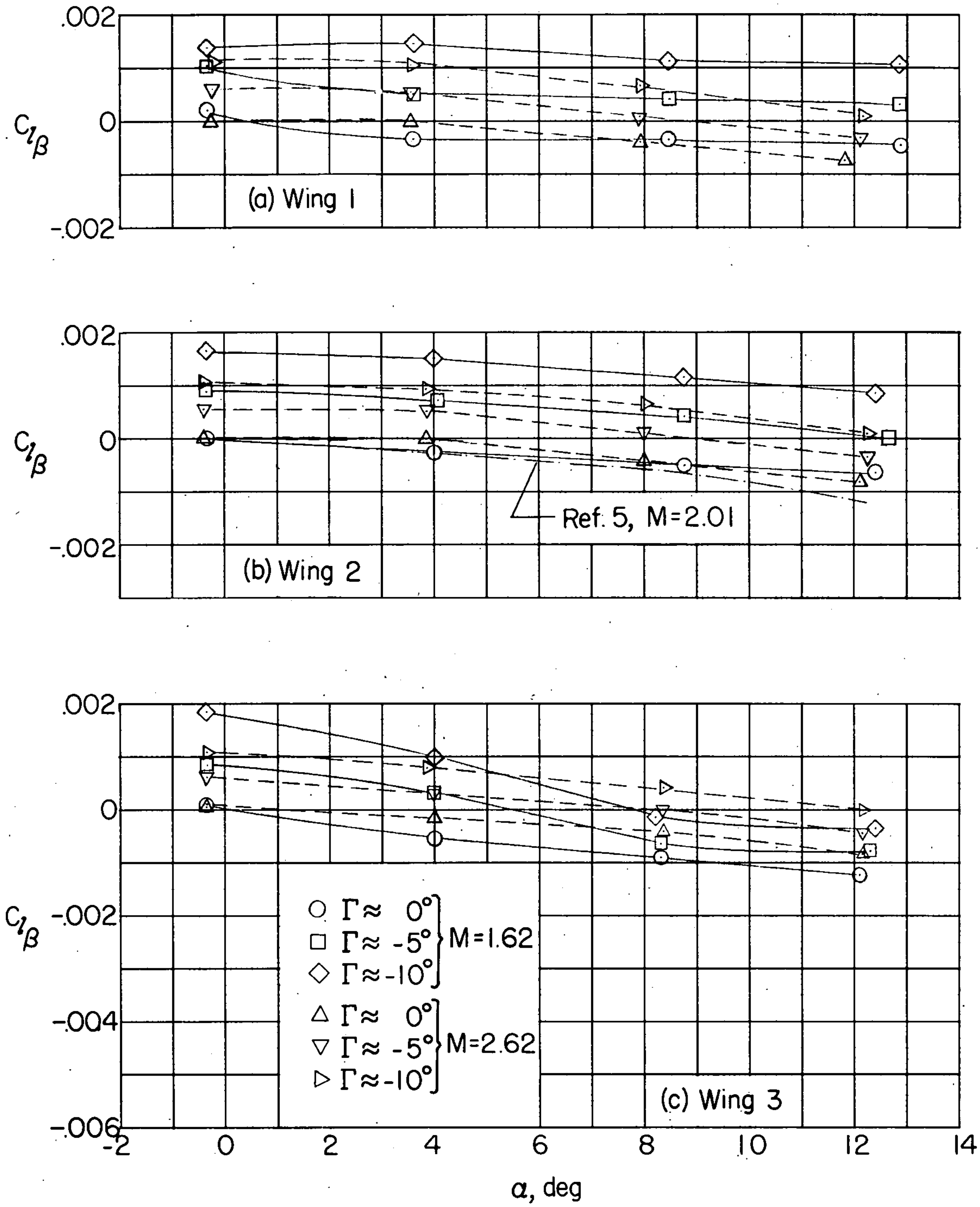

Figure 20.- Variation of C_{l_β} with α for the wing-body combinations.

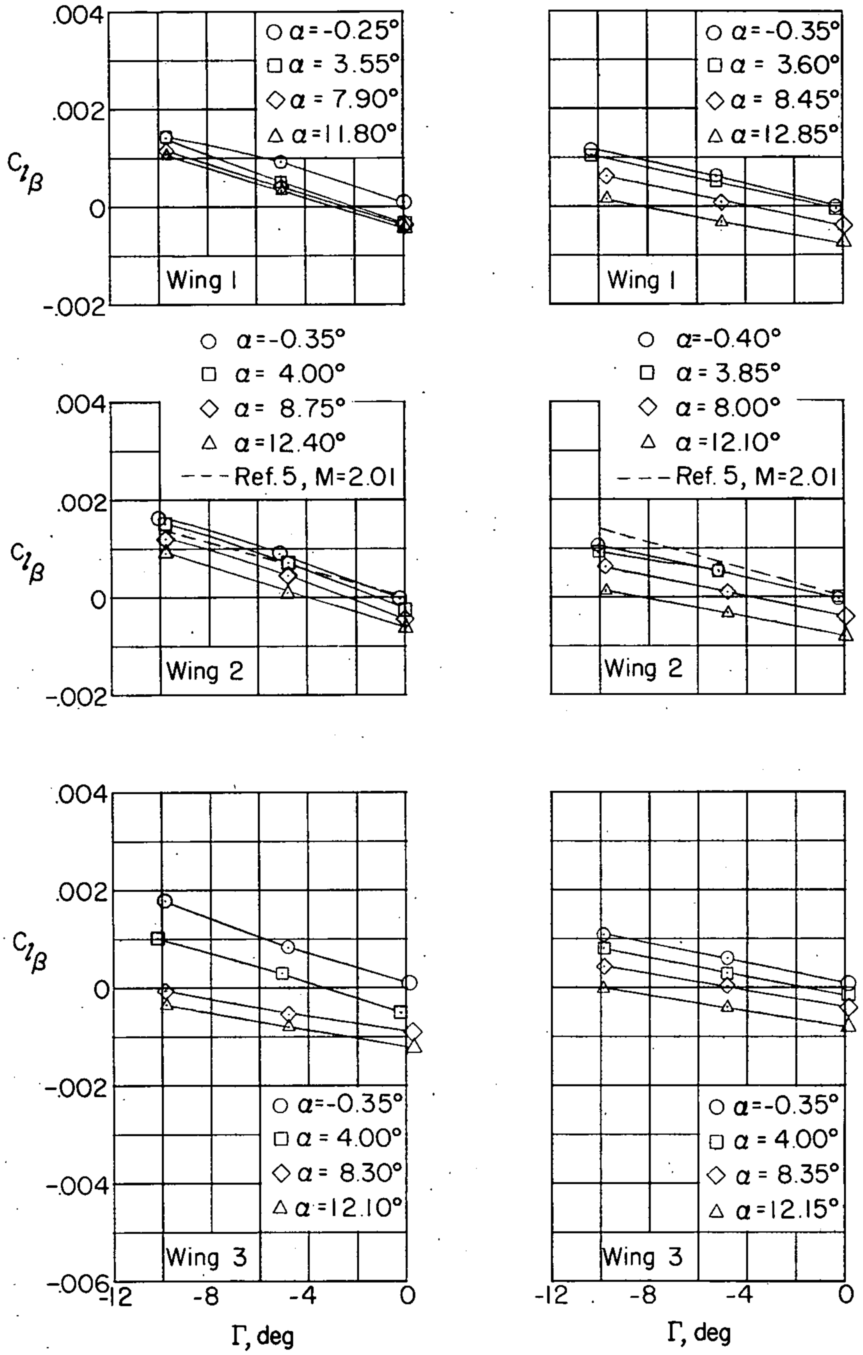

(a) M = 1.62. (b) M = 2.62.

Figure 21.- Variation of C_{l_β} with Γ for the wing-body combinations.

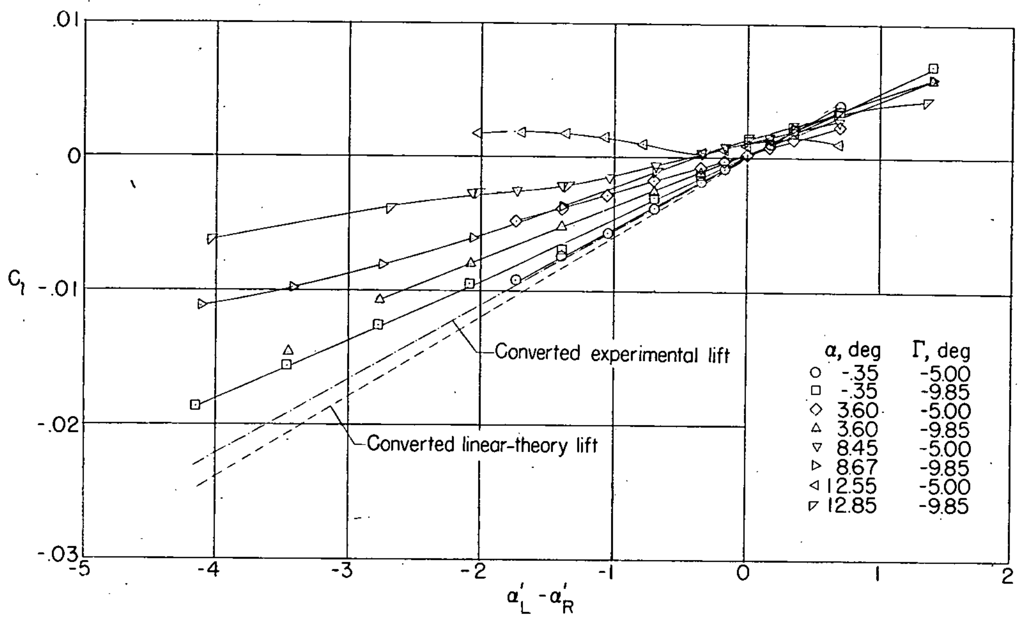

(a) M = 1.62.

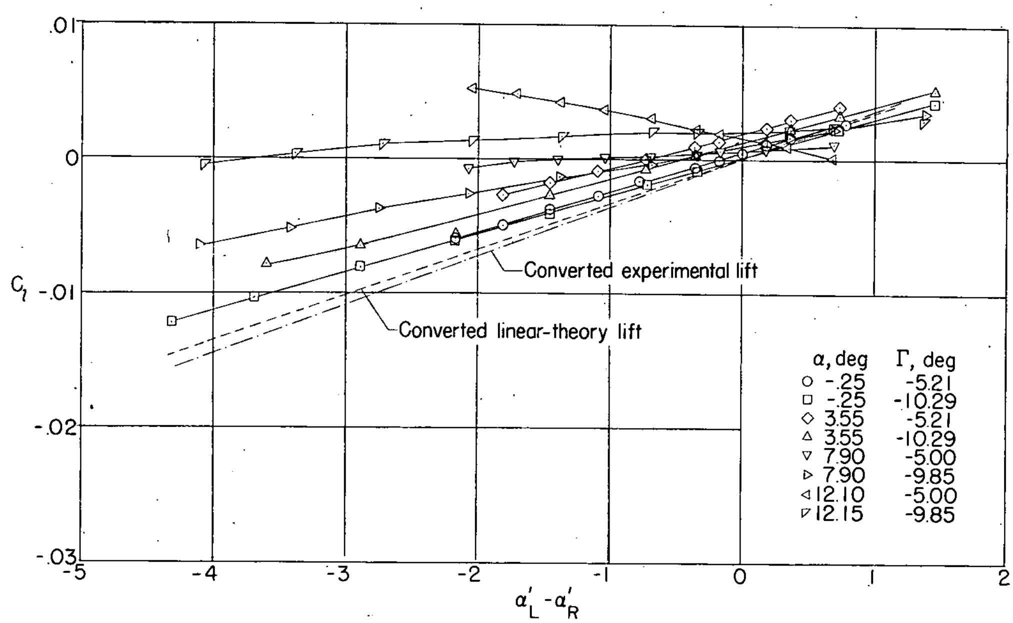

(b) M = 2.62.

Figure 22.- Variation of C_l with true differential panel angle of attack for combined angles of sideslip, angles of attack, and dihedral angles. Wing 1.

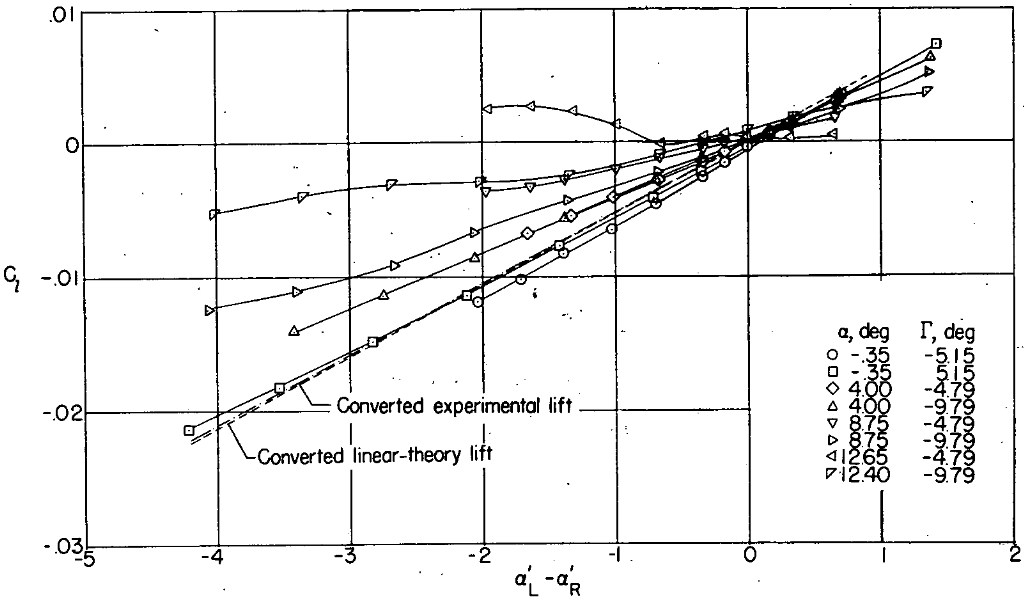

(a) M = 1.62.

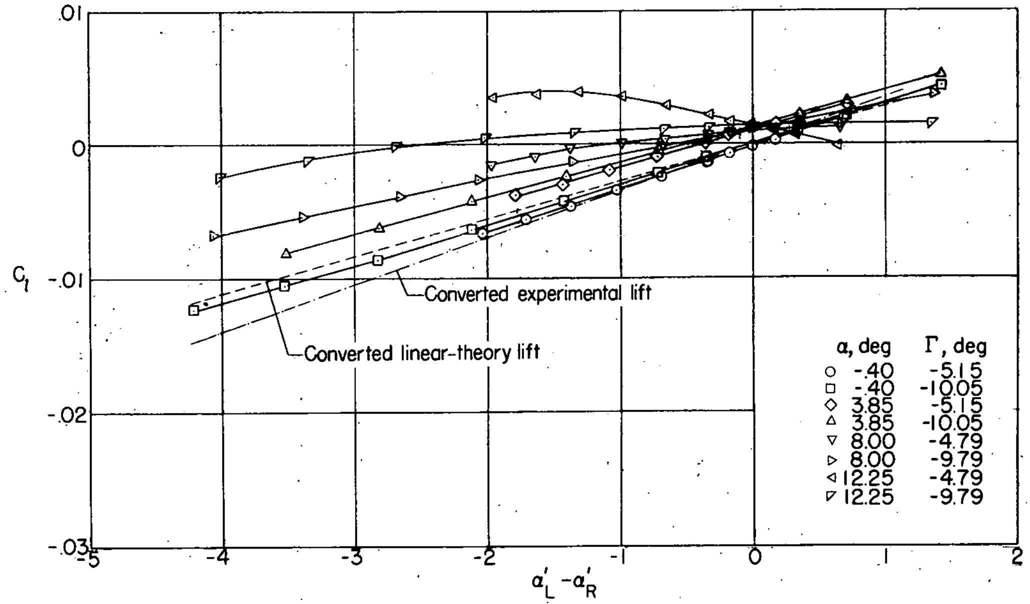

(b) M = 2.62.

Figure 23.- Variation of C_l with true differential panel angle of attack for combined angles of sideslip, angles of attack, and dihedral angles. Wing 2.

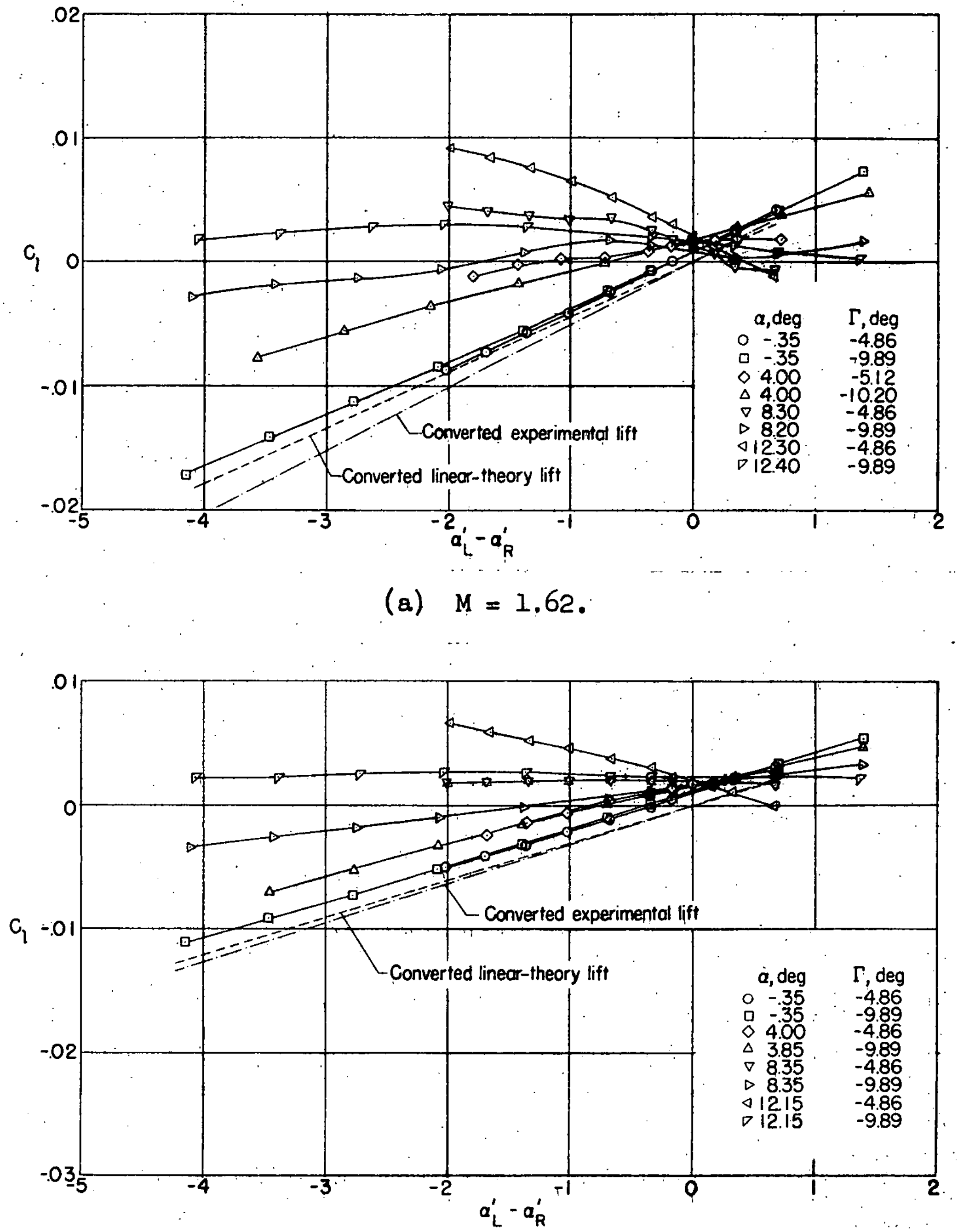

(a) M = 1.62.

(b) M = 2.62.

Figure 24.- Variation of C_l with true differential panel angle of attack for combined angles of sideslip, angles of attack, and dihedral angles. Wing 3.